TE DIFFRACTION BY A PAIR OF SEMI-INFINITE MATERIAL SHEETS

John L. Volakis
Radiation Laboratory
Department of Electrical Engineering and Computer Science
The University of Michigan
Ann Arbor, MI 48109-2122

Abstract

The extended spectral ray method (ESRM) is employed in deriving expressions for the multiply diffracted fields by a pair of semi-infinite parallel material sheets/layers. One of the sheets is chosen to satisfy a second order boundary condition simulating a thin dielectric layer and the other is a resistive sheet. Of interest is the computation of the leading edge scattering given as the sum of the singly and multiply diffracted fields with particular attention given to the computation of higher order diffraction fields beyond the second. Their evaluation required a non-traditional approach and up to fifth order diffraction fields are derived and applied in computing the scattering by a pair of half sheets simulating a metal-backed dielectric half plane as thin as 1/20 of a wavelength. Numerical results for other practical simulations are presented and compared with results based on alternative computational methods, where applicable.

TABLE OF CONTENTS

I. INTRODUCTION

Of interest in recent years has been the electromagnetic characterization of material geometries. In this report we consider the problem of diffraction by a pair of parallel material half sheets as shown in Fig. 1. Specifically, the upper half sheet satisfies a second order boundary conditions [1,2] simulating a thin dielectric layer having arbitrary constitutive parameters. The lower half sheet satisfies the resistive sheet boundary condition [3]. Diffraction coefficients for each of these half sheets in isolation are already available and, therefore, a goal in this report is to determine the interaction fields between the two half sheets.

The determination of the interaction or multiple diffracted fields is accomplished here via the extended spectral ray method (ESRM) [4-6]. The ESRM technique has been employed, rather successfully, in the past [5-7] for the prediction of the multiple interaction fields among edges at a distance much less than a wavelength. Particularly, in the case of backscatter by a resistive/dielectric strip [5], the third order ESRM solution remained accurate for strip widths down to 1/8 of a wavelength or less. Similar observations hold for the backscatter by a thick impedance edge [6]. In both of these cases, however, the ray paths associated with higher order mechanisms did not traverse along shadow or reflection boundaries. As illustrated in Fig. 2, this is a particular characteristic of the multiple diffraction mechanisms (beyond the third) associated with the subject geometry. Because of it, their treatment within the framework of the ESRM requires a deviation from the usual approach and is the main contribution of this report.

Of interest in this report is also the treatment of the diffraction by a thin truncated layer backed by a resistive half sheet as shown in Fig. 3. An exact treatment of this problem leads to a pair of coupled integral equations that cannot be decoupled. It is, therefore, of interest to pursue a high frequency solution. Since the thin dielectric layer can be modeled by a current sheet satisfying a second order boundary condition at the center of the layer [1, 2], the configuration in Fig. 3 can be modeled by a pair of parallel half sheets (see Fig. 1) in close proximity. Based on experience, the ESRM should be capable of providing a good simulation when a sufficient number of multiply diffracted fields are included in the analysis. For this purpose, up to and including quintuply diffracted fields are derived for the pair of half sheets shown in Fig. 1

Our primary attention throughout the report is the determination of the leading edge scattering by the pair of (penetrable) half sheets. Specifically, the observation and scattering directions will be restricted in the range $\pi/2 < \phi\ 3\pi/2$. Since the half sheets are penetrable, this restriction allows one to avoid at this time the treatment of possible contributions from modal fields within the material.

In the following, a mathematical description of the half sheets and their diffracted fields in isolation are first given for reference purposes. Next, the development of uniform diffraction coefficients for the doubly, triply, quadruply and quintuply diffracted fields is presented. Except for the doubly diffracted fields, those contributed by the higher order mechanisms require a non-traditional treatment because they include ray paths traversing along reflection boundaries. The last section of the report presents results which validate the uniformity and continuity of the total field as well as the accuracy and limitations of the solution.

II. SHEET BOUNDARY CONDITIONS

Consider a pair of half-sheets, as shown in Figure 1, illuminated by the plane wave

$$H_z^i = e^{jk\,(x\cos\phi_o + y\sin\phi_o)} \qquad (1)$$

The upper half plane satisfies the boundary conditions [1, 2]

$$\frac{Y}{\eta_e}(E_x^+ + E_x^-) = H_z^+ - H_z^-$$

$$Z\left(\frac{1}{\eta_m^*} + \frac{1}{\eta_e^*}\right)(H_z^+ + H_z^-) - \frac{1}{jk\eta_e^*}\frac{\partial}{\partial y}(E_x^+ + E_x^-) = E_x^+ - E_x^- \qquad (2)$$

where ± imply the field values above and below the sheet, Z = 1/Y is the free space intrinsic impedance and

$$\eta_e = \frac{-2j}{k\tau\,(\varepsilon-1)} \quad , \qquad \eta_m^* = \frac{-2j}{k\tau\,(\mu-1)} \quad , \qquad \eta_e^* = \frac{-2j\varepsilon}{k\tau\,(\varepsilon-1)} \quad . \tag{3}$$

As such, (2) represents a simulation of a dielectric layer of thickness τ having relative constitutive parameters (ε, μ) and centered at $y = 0$.

The lower half sheet at $y = -w$ satisfies the resistive sheet boundary condition [3]

$$E_x^+ + E_x^- = 2R\,(H_z^+ - H_z^-)$$

$$E_x^+ = E_x^- \tag{4}$$

where again the $\pm$ imply the field values above and below the resistive sheet and R denotes the resistivity of the sheet.

Of interest is the evaluation of the diffracted fields in the presence of the excitation (1). Restricting the angles of incidence and diffraction in the range $\pi/2 < \phi, \phi_o < 3\pi/2$, the total diffracted field is then given as the the sum of the contributions by the single and multiple diffraction mechanisms among the pair of edges Q_1 and Q_2 formed by the half sheets. For impenetrable sheets, such as a pair of impedance or perfectly conducting half planes, a solution in some spatial range is directly extendable to another. Unfortunately, this is not the case with the penetrable sheets considered here and, therefore, such a restriction is necessary.

Below we begin the evaluation of the multiple diffracted fields with particular emphasis in the derivation of expressions applicable to diffraction mechanisms beyond the second. Since our goal is to generate a solution that remains accurate for small sheet separation distances, say down to 1/20 of a wavelength, expressions are derived up to and including the quintuply diffracted fields.

III. SINGLY DIFFRACTED FIELDS

The diffracted field by the upper half sheet in isolation is given by [7]

$$H_{z1}(\phi_1\phi_0) = \frac{j}{4\pi} \int_{S(0)} \left[\sec\left(\frac{\alpha \pm \phi \mp \phi_o}{2}\right) + \sec\left(\frac{\alpha \pm \phi \pm \phi_o}{2}\right) \right] \left[H_z^e(\alpha + \gamma, \phi_o) \pm H_z^m(\alpha + \gamma, \phi_o) \right] e^{-jk\rho\cos\alpha}\, d\alpha \;; \quad y \gtrless 0 \tag{5}$$

where

$$H_z^e(\alpha, \phi_o) = \eta_1\, K_+(\alpha, \eta_1)\, K_+(\phi_o, \eta_1) \tag{6}$$

$$H_z^m(\alpha, \phi_0) = -\left[\frac{\eta^*}{\eta_m^* \sin\alpha \sin\phi_0} - \frac{\eta^*}{\eta_e^* \tan\alpha \tan\phi_0} \right] K_+(\alpha, \eta_1^*)\, K_+(\phi_0, \eta_1^*)\, K_+(\alpha, \eta_2^*)\, K_+(\phi_o, \eta_2^*) \tag{7}$$

in which $K_+(\phi, \eta)$ is the Wiener-Hopf split function explicitly defined in [7, 8] (note that in [7] the first argument of K_+ is $\cos\alpha$ rather than α as employed here),

$$\eta_1 = \frac{1}{\eta_e} \,, \qquad \frac{1}{\eta^*} = \frac{1}{\eta_e^*} + \frac{1}{\eta_m^*} \tag{8}$$

and

$$\eta_{1,2}^* = \frac{\eta^*}{2}\left[1 \pm \sqrt{1 + \left(\frac{4}{\eta^* \eta_e^*}\right)} \right] . \tag{9}$$

Also,

$$\gamma = \begin{cases} \phi & y > 0 \\ 2\pi - \phi & y < 0 \ . \end{cases}$$

and (ρ, ϕ) are the usual cylindrical coordinates of the observation point.

A non-uniform expression $(\rho \rightarrow \infty)$ for H_{z1} is

$$H_{z1}(\phi, \phi_o) \sim - \frac{e^{-j\pi/4}}{2\sqrt{2\pi k}} \left[\sec\left(\frac{\phi+\phi_o}{2}\right) + \sec\left(\frac{\phi-\phi_o}{2}\right) \right] \left[H_z^e(\phi, \phi_o) + H_z^m(\phi, \phi_o) \right] \frac{e^{-jk\rho}}{\sqrt{\rho}}$$

$$\sim D_1(\phi, \phi_o) \frac{e^{-jk\rho}}{\sqrt{\rho}} \tag{10a}$$

since $K_+(\phi, \eta) = K_+(2\pi - \phi, \eta)$, where $D_1(\phi_1, \phi_0)$ is the diffraction coefficient for the singly diffracted fields from Q_1. The above is, of course, invalid near the reflection and shadow boundaries occuring at $\phi \approx \pi \pm \phi_0$, where a uniform evaluation [9] of (5) is necessary. In so doing, at the reflection boundary we find

$$H_{z1}(\phi \approx \pi - \phi_0, \phi_0) \sim \left[\frac{1}{2} - \frac{e^{-j\pi/4}}{2\sqrt{2\pi k\rho}} \sec\left(\frac{\phi - \phi_0}{2}\right) \right] e^{-jk\rho} \left[H_z^e(\phi, \phi_0) + H_z^m(\phi, \phi_0) \right] \tag{10b}$$

in which the first term in the brackets is equal to one-half the reflected field by the planar sheet. Clearly, (10b) implies that at $\phi \approx \phi_o \approx \pi/2$, the diffracted field can be decomposed into a plane wave and a slowly varying cylindrical wave. In contrast, the sum of the two waves yields a rapidly varying field whose treatment cannot be handled via the ESRM for the computation of the multiply diffracted fields.

The diffracted field by the resistive half sheet in isolation is given by [5]

$$H_{z2}(\phi, \phi_o) = \frac{j}{4\pi} \eta_{1R} \int_{S(0)} \left[\sec\left(\frac{\alpha \pm \phi \quad \phi_o}{2} \right) + \sec\left(\frac{\alpha \pm \phi \pm \phi_o}{2} \right) \right] K_+(\alpha + \gamma, \eta_{1R})\, K_+(\phi_o, \eta_{1R}) \cdot$$

$$\cdot \; e^{-jk\rho_2 \cos\alpha}\, d\alpha \tag{11}$$

in which

$$\eta_{1R} = Z/2R \ . \tag{12}$$

Note also that in the far zone $\rho_2 = \rho + w\cos\phi$. A non-uniform evaluation of (11) now yields

$$H_{z2}(\phi, \phi_o) \sim -\frac{e^{-j\pi/4}}{2\sqrt{2\pi k}} \left[\sec\left(\frac{\phi + \phi_o}{2} \right) + \sec\left(\frac{\phi - \phi_o}{2} \right) \right] \eta_{1R} K_+(\phi, \eta_{1R})\, K_+(\phi_o, \eta_{1R}) \frac{e^{-jk\rho_2}}{\sqrt{\rho_2}}$$

$$\sim D_2(\phi, \phi_o) \frac{e^{-kj\rho_2}}{\sqrt{\rho_2}} \ , \tag{13a}$$

where $D_2(\phi, \phi_0)$ is again identified as the diffraction coefficient for this mechanism. As before,

when $\phi \approx \pi - \phi_0$, we find that

$$H_{z2}(\phi \approx \pi - \phi_0, \phi_0) \sim \left[\frac{1}{2} - \frac{e^{-j\pi/4}}{2\sqrt{2\pi k\rho}} \sec\left(\frac{\phi - \phi_0}{2} \right) \right] \eta_{1R}\ K_+(\phi, \eta_{1R})\, K_+(\phi_0, \eta_{1R})\, e^{-jk\rho_2}$$

$$\sim -\frac{e^{-j\pi/4}}{2\sqrt{2\pi k\rho}} \left\{ -\sqrt{2\pi k\rho}\ e^{j\pi/4} + \sec\left(\frac{\phi - \phi_o}{2} \right) \right\} \eta_{1R} K_+(\phi, \eta_{1R})\, K_+(\phi_o, \eta_{1R})\, e^{-jk\rho_2} \tag{13b}$$

allowing a decomposition of the diffracted field into a plane wave and a slowly varying cylindrical wave.

IV. DOUBLY DIFFRACTED FIELD

Double diffraction occurs when the plane wave after diffraction from the top (bottom) half sheet propagates towards and diffracts from the bottom (top) half sheet as illustrated in Figure 4. The diffracted field from the top edge (Q_1) toward the bottom edge (Q_2) is, of course, given by the integral (5) with $\phi = \pi/2$ and $\rho = w$. But in accordance with the ESRM (see Figure 4b) this integral can be interpreted as a sum of inhomogeneous plane waves emanating from Q_1 at an angle $3\pi/2 + \alpha$, where α is the angle measured from the stationary ray [10]. Each of the inhomogeneous plane waves will then be incident on the bottom edge at an angle $\pi/2 + \alpha$ with respect to its top face. For far zone observations, their individual contributions are given by (13a) and, therefore, an integral expression for the doubly diffracted field from Q_1 to Q_2 is

$$H_{z21}(\phi, \phi_o) = \Delta_1 \int_{S(0)} \left[\sec\left(\frac{\alpha - 3\pi/2 + \phi_o}{2}\right) + \sec\left(\frac{\alpha - 3\pi/2 - \phi_o}{2}\right) \right]$$

$$\left[\sec\left(\frac{\alpha + \pi/2 + \phi}{2}\right) + \sec\left(\frac{\alpha + \pi/2 - \phi}{2}\right) \right] F(\alpha, \phi, \phi_o)\, e^{-jkw\cos\alpha}\, d\alpha \qquad (14)$$

in which

$$\Delta_1 = \sqrt{\frac{k}{2\pi}}\, e^{-j\,\pi/4}\, \frac{e^{-jk\rho_2}}{\sqrt{\rho}} = \Delta\, e^{-jkw\sin\phi} \qquad (15)$$

and

$$F(\alpha, \phi, \phi_o) = \left(\frac{e^{-j\,\pi/4}}{2\sqrt{2\pi k}} \right)^2 \left[H_z^e(\alpha + \pi/2, \phi_o) - H_z^m(\alpha + \pi/2, \phi_o) \right] \eta_{1R}\, K_+(\phi, \eta_{1R})\, K_+(\alpha + \pi/2, \eta_{1R}) \tag{16}$$

From (14), it is clear that $H_{z21}(\phi, \phi_o)$ can be written as a sum of four integrals

$$H_{z21}(\phi, \phi_o) = I^I\left(\frac{3\pi}{2} - \phi_o, -\frac{\pi}{2} - \phi\right) + I^I\left(\frac{3\pi}{2} - \phi_o, -\frac{\pi}{2} + \phi\right) + I^I\left(\frac{3\pi}{2} + \phi_o, -\frac{\pi}{2} - \phi\right) +$$
$$+ I^I\left(\frac{3\pi}{2} + \phi_0, -\frac{\pi}{2} + \phi\right) \tag{17}$$

where

$$I^I(\alpha_i, \alpha_j) = \Delta_1 \int_{S(0)} F(\alpha, \phi, \phi_o) \sec\left(\frac{\alpha - \alpha_i}{2}\right) \sec\left(\frac{\alpha - \alpha_j}{2}\right) e^{-jkw\cos\alpha}\, d\alpha \tag{18a}$$

whose asymptotic evaluation yields

$$I^I(\alpha_i, \alpha_j) \sim I(\alpha_i, \alpha_j)\, F(0, \phi, \phi_0)\, \frac{e^{-jkw}}{\sqrt{w}} \frac{e^{-jk\rho_2}}{\sqrt{\rho}}. \tag{18b}$$

A uniform expression for $I(\alpha_i, \alpha_j)$ that accounts for the case when a_i and/or a_j are near the saddle point is [9, 10]

$$I(\alpha_i, \alpha_j) = \sec\frac{\alpha_i}{2} \sec\frac{\alpha_j}{2} \frac{a_i a_j}{a_j - a_i} \left[\frac{F_{kp}(kwa_i)}{a_i} - \frac{F_{kp}(kwa_j)}{a_j} \right] \tag{19a}$$

provided $\alpha_i \neq \alpha_j$. Alternatively, if $\alpha_i = \alpha_j$ then a suitable expression for $I(\alpha_i, \alpha_j)$ is

$$I(a_i, a_i) = \sec^2 \frac{a_i}{2} \left\{ -jkwa_i \left[F_{kp}(kwa_i) - 1 \right] + \frac{1}{2} F_{kp}(kwa_i) \right\} \tag{19b}$$

In (19a) and (19b),

$$a_i = 2\cos^2\frac{\alpha_i}{2} \tag{20}$$

and

$$F_{kp}(z^2) = 2j\sqrt{z}\, e^{jz}\int_{\sqrt{z}}^{\infty} e^{-jt^2}\,dt \tag{21}$$

is the UTD transition function whose properties are discussed in [9].

The double diffraction coefficient $D_{21}(\phi, \phi_o)$ is now determined in accordance with the relation

$$H_{z21}(\phi, \phi_o) \sim D_{21}(\phi, \phi_o)\frac{e^{-jk\rho_2}}{\sqrt{\rho}} = D_{21}(\phi, \phi_o)\frac{e^{-jk\rho}}{\sqrt{\rho}}e^{-jkw\sin\phi} \tag{22}$$

together with (17)-(19). By invoking reciprocity, the doubly diffracted field traversing from Q_2 to Q_1 (see Fig. 4c) is simply given by

$$H_{z12}(\phi, \phi_o) \sim D_{12}(\phi, \phi_o)\frac{e^{-jk\rho}}{\sqrt{\rho}}e^{-jkw\sin\phi_o} = D_{21}(\phi_o, \phi)\frac{e^{-jk\rho}}{\sqrt{\rho}}e^{-jkw\sin\phi_o} \tag{23}$$

and this completes the analysis for the doubly diffracted fields.

V. TRIPLY DIFFRACTED FIELD

The mechanisms associated with the triply diffracted field are illustrated in Figure 5.

Let us first consider the mechanism shown in Figure 5a. In this case the plane wave incident onto Q_1 generates spectral waves that are in turn incident upon Q_2 at an angle $\pi/2 + \alpha$ to subsequently undergo a double diffraction before returning to the observer. Accordingly, an integral expression for the contribution of this mechanism is

$$H_{z121}(\phi, \phi_o) = \Delta \int_{S(0)} \left[\sec\left(\frac{\alpha - 3\pi/2 + \phi_o}{2}\right) + \sec\left(\frac{\alpha - 3\pi/2 - \phi_o}{2}\right) \right] \left(- \frac{e^{-j\pi/4}}{2\sqrt{2\pi k}} \right)$$

$$\left[H_z^e(\alpha + \pi/2, \phi_o) - H_z^m(\alpha + \pi/2, \phi_o) \right] D_{12}(\phi, \pi/2 + \alpha)\, e^{-jkw\cos\alpha}\, d\alpha \qquad (24)$$

where $D_{12}(\phi, \pi/2 + \alpha) = D_{21}(\pi/2 + \alpha, \phi)$ is the double diffraction coefficient defined in (17) - (23). Of importance in the evaluation of (24) is, of course, the integrand value at and near the saddle point $\alpha = 0$. We, thus, require $D_{12}(\phi, \pi/2)$. However, expression (19) becomes non-uniform with respect to ϕ when $\phi \approx \pi/2$ and is thus invalid, unless w is large. Rewriting $D_{12}(\phi, \pi/2)$ as

$$D_{12}(\phi, \beta) = D_{12}^{I}(\phi, \beta) + D_{12}^{II}(\phi, \beta) \qquad (25)$$

with

$$D_{12}^{I}(\phi, \beta) = \left[I\left(\frac{3\pi}{2} - \phi, -\frac{\pi}{2} - \beta\right) + I\left(\frac{3\pi}{2} - \phi, -\frac{\pi}{2} + \beta\right) \right] F(0, \beta, \phi) \frac{e^{-jkw}}{\sqrt{w}} \qquad (26)$$

$$D_{12}^{II}(\phi, \beta) = \left[I\left(\frac{3\pi}{2} + \phi, -\frac{\pi}{2} - \beta\right) + I\left(\frac{3\pi}{2} + \phi, -\frac{\pi}{2} + \beta\right) \right] F(0, \beta, \phi) \frac{e^{-jkw}}{\sqrt{w}}, \qquad (27)$$

we observe that $D^I_{12}(\phi, \beta)$ is the invalid portion of $D_{12}(\phi, \beta)$ when $\beta \approx \frac{\pi}{2}$. To find a valid expression for $D^I_{12}(\phi, \frac{\pi}{2})$ we return to the scenario associated with the triply diffracted field shown in Figure 5a.

The spectral plane wave emanating from Q_1 is incident upon Q_2 at an angle $\pi/2 + \alpha$. Most of the scattering from Q_2 will then be near the specular direction $\pi/2 - \alpha$, but if $\alpha \approx 0$, Q_1 will be in the path of the specular return and the diffracted field from Q_2 will be given by (13b) with $\rho = w$ if evaluated at Q_1. That is, the diffracted field from Q_2 consists of a plane wave portion equal to one-half the reflected field plus a slowly varying cylindrical wave. The plane wave portion of $H_{z2}(\pi/2 + \alpha, \pi/2 - \alpha)$ is obviously that associated with $D^I_{12}(\phi, \pi/2)$. At Q_1, the plane wave portion of $H_{z2}(\pi/2 + \alpha, \pi/2 - \alpha)$ has the value

$$\frac{1}{2}\eta_{1R} K_+^2(\pi/2, \eta_{1R})\, e^{-jkw}$$

and makes an angle $3\pi/2 - \alpha$ with respect to the top face at Q_1. Thus, an appropriate far zone expression for $D^I_{12}(\phi, \pi/2)$ is

$$D^I_{12}(\phi, \frac{\pi}{2} + \alpha)\Big|_{\alpha \approx 0} \approx \frac{1}{2}\eta_{1R} K_+^2(\frac{\pi}{2}, \eta_{1R})\, e^{-jkw} D_1(\phi, \frac{3\pi}{2} - \alpha)$$

$$= -\sqrt{2\pi k w}\, e^{j\pi/4}\left[\sec\left(\frac{3\pi/2 - \alpha + \phi}{2}\right) + \sec\left(\frac{3\pi/2 - \alpha - \phi}{2}\right)\right] F(0, \frac{\pi}{2} + \alpha, \phi)\, \frac{e^{-jkw}}{\sqrt{w}}$$

(28)

By comparison with (26), we thus observe that

$$I(\alpha_1, -\pi+\alpha)\Big|_{\phi\approx\frac{\pi}{2}} \rightarrow -\sqrt{2\pi k w}\; e^{j\pi/4} \sec\left(\frac{\alpha_1-\alpha}{2}\right) \tag{29}$$

for $\alpha \approx 0$, a result that will prove useful in simplifying the analysis associated with higher order diffraction mechanisms.

Substituting (25) along with (27) and (28) into the triple diffraction integral (24) and performing a uniform evaluation as in the double diffraction case yields

$$H_{z121}(\phi,\phi_o) \sim D_{121}(\phi,\phi_o)\frac{e^{-jk\rho}}{\sqrt{\rho}}$$

$$= \left\{-\sqrt{2\pi k w}\; e^{j\pi/4}\left[I\left(\frac{3\pi}{2}-\phi, \frac{3\pi}{2}-\phi_o\right) + I\left(\frac{3\pi}{2}-\phi, \frac{3\pi}{2}+\phi_o\right)\right.\right.$$

$$\left. + I\left(\frac{3\pi}{2}+\phi, \frac{3\pi}{2}-\phi_o\right) + I\left(\frac{3\pi}{2}+\phi, \frac{3\pi}{2}+\phi_o\right)\right] + \left[I\left(\frac{3\pi}{2}-\phi_o, 0\right) + I\left(\frac{3\pi}{2}+\phi_o, 0\right)\right]$$

$$\left.\left[I\left(\frac{3\pi}{2}-\phi, 0\right) + I\left(\frac{3\pi}{2}+\phi, 0\right)\right]\right\}\left(\frac{e^{-jkw}}{\sqrt{w}}\right)^2 F_3(0,\phi,\phi_o)\frac{e^{-jk\rho}}{\sqrt{\rho}} \tag{30}$$

with $I(\alpha_i, \alpha_j)$ as defined in (19),

$$F_3(0,\phi,\phi_o) = -\frac{e^{-j\pi/4}}{2\sqrt{2\pi k}}\left[H_z^e\left(\frac{\pi}{2},\phi_o\right) - H_z^m\left(\frac{\pi}{2},\phi_o\right)\right] F\left(0,\frac{\pi}{2},\phi\right) \; . \tag{31}$$

and $F(0, \pi/2, \phi)$ as given in (16).

The triply diffracted field whose ray scenario is shown in Figure 5b can be obtained in a parallel manner. We find

$$H_{z212}(\phi, \phi_o) \sim D_{212}(\phi, \phi_o) \frac{e^{-jk\rho}}{\sqrt{\rho}} e^{-jkw(\sin\phi + \sin\phi_o)}$$

$$= \Big\{ -\sqrt{2\pi kw}\, e^{j\pi/4} \Big[I(-\tfrac{\pi}{2} - \phi, -\tfrac{\pi}{2} - \phi_o) + I(-\tfrac{\pi}{2} - \phi, -\tfrac{\pi}{2} + \phi_o) + I(-\tfrac{\pi}{2} + \phi, -\tfrac{\pi}{2} - \phi_o)$$

$$+ I(-\tfrac{\pi}{2} + \phi, -\tfrac{\pi}{2} + \phi_o) \Big] + \Big[I(-\tfrac{\pi}{2} - \phi_o, 0) + I(-\tfrac{\pi}{2} + \phi_o, 0) \Big] \Big[I(-\tfrac{\pi}{2} - \phi, 0) + I(-\tfrac{\pi}{2} + \phi, 0) \Big] \Big\}$$

$$\cdot \left(\frac{e^{-jkw}}{\sqrt{w}} \right)^2 F'_3(0, \phi, \phi_o) \frac{e^{-jk\rho}}{\sqrt{\rho}} e^{-jkw(\sin\phi + \sin\phi_o)} \quad (32)$$

in which

$$F'_3(0, \phi, \phi_o) = -\frac{e^{-j\pi 4}}{2\sqrt{2\pi k}} \eta_{1R} K_+(\tfrac{\pi}{2}, \eta_{1R}) K_+(\phi_o, \eta_{1R}) F(0, \phi, \tfrac{3\pi}{2}). \quad (33)$$

and $D_{212}(\phi, \phi_0)$ is the diffraction coefficient for this mechanism.

VI. QUADRUPLY DIFFRACTED FIELDS

The two mechanisms associated with the quadruply diffracted fields are illustrated in Figure 6 and as in the double diffraction case they are reciprocal. Let us first consider the evaluation of $H_{z2121}(\phi, \phi_0)$. In this case the plane wave incident upon Q_1 generates spectral waves which are in turn incident upon Q_2 at an angle $\pi/2 + \alpha$ with respect to the upper face of the lower sheet. Each of the plane waves subsequently undergoes a triple diffraction before returning to the observer. An appropriate integral expression for this quadruply diffracted field then is

$$H_{z2121}(\phi,\phi_o) = \Delta\, e^{-jkw\sin\phi} \int_{S(0)} \left[\sec\left(\frac{\alpha - 3\pi/2 + \phi_o}{2}\right) + \sec\left(\frac{\alpha - 3\pi/2 - \phi_o}{2}\right) \right] \left(- \frac{e^{-j\pi/4}}{2\sqrt{2\pi k}} \right)$$

$$\left[H_z^e\left(\alpha + \frac{\pi}{2}, \phi_o\right) - H_z^m\left(\alpha + \frac{\pi}{2}, \phi_o\right) \right] D_{212}\left(\phi, \frac{\pi}{2} + \alpha\right) e^{-jkw\cos\alpha}\, d\alpha \qquad (34)$$

and in view of (29), the triple diffraction coefficient $D_{212}(\pi/2 + \alpha, \phi)$ is given by

$$D_{212}\left(\frac{\pi}{2} + \alpha, \phi\right) = \Bigg\{ - \sqrt{2\pi kw}\, e^{j\pi/4} \left\{ I\left(-\frac{\pi}{2} - \phi, \alpha\right) + I\left(-\frac{\pi}{2} - \phi, \alpha\right) + \right.$$

$$\left. - \sqrt{2\pi kw}\, e^{j\pi/4} \left[\sec\left(\frac{-\pi/2 - \phi + \alpha}{2}\right) + \sec\left(\frac{-\pi/2 + \phi + \alpha}{2}\right) \right] \right\}$$

$$+ \left[I(-\pi - \alpha, 0) + I(\alpha, 0) \right] \left[I\left(-\frac{\pi}{2} - \phi, 0\right) + I\left(-\frac{\pi}{2} + \phi, 0\right) \right] \Bigg\} \left(\frac{e^{-jkw}}{\sqrt{w}} \right)^2 F'_3\left(0, \phi, \frac{\pi}{2} + \alpha\right)$$

$$(35)$$

for $\alpha \approx 0$.

Performing a uniform evaluation of (34) yields

$$H_{z2121}(\phi,\phi_o) = \Bigg[- \sqrt{2\pi kw}\, e^{j\pi/4} \left\{ I\left(\frac{3\pi}{2} - \phi_o, 0\right) + I\left(\frac{3\pi}{2} + \phi_o, 0\right) \right\} \left\{ I\left(-\frac{\pi}{2} - \phi, 0\right) + I\left(-\frac{\pi}{2} + \phi, 0\right) \right\}$$

$$+ j2\pi kw \left\{ I\left(-\frac{\pi}{2} - \phi, \frac{3\pi}{2} - \phi_o\right) + I\left(-\frac{\pi}{2} - \phi, \frac{3\pi}{2} + \phi_o\right) + I\left(-\frac{\pi}{2} + \phi, \frac{3\pi}{2} - \phi_o\right) + I\left(-\frac{\pi}{2} + \phi, \frac{3\pi}{2} + \phi_o\right) \right\}$$

$$+ \left[- \sqrt{2\pi kw}\, e^{j\pi/4} \left\{ I_1\left(\frac{3\pi}{2} - \phi_o\right) + I_1\left(\frac{3\pi}{2} + \phi_o\right) \right\} + I(0,0) \left\{ I\left(\frac{3\pi}{2} - \phi_o, 0\right) + I\left(\frac{3\pi}{2} + \phi_o, 0\right) \right\} \right]$$

$$\cdot\left\{ I\left(-\frac{\pi}{2}-\phi, 0\right) + I\left(-\frac{\pi}{2}+\phi, 0\right)\right\}\Bigg]\left(\frac{e^{-jkw}}{\sqrt{w}}\right)^3 F_4(0, \phi, \phi_o)\,\frac{e^{-jk\rho}}{\sqrt{\rho}}e^{-jkw\,\sin\phi} \tag{36}$$

in which

$$I_1(\alpha_i) = \sec\frac{\alpha_i}{2}\,F_{kp}(kwa_i) \tag{37}$$

and

$$F_4(0, \phi, \phi_o) = -\frac{e^{-j\pi/4}}{2\sqrt{2\pi k}}\left[H_z^e\left(\frac{\pi}{2}, \phi_o\right) - H_z^m\left(\frac{\pi}{2}, \phi_o\right)\right]F_3'\left(0, \phi, \frac{\pi}{2}\right) \;. \tag{38}$$

where $F'_3(0, \phi, \phi_0)$ is defined in (33). Also, by invoking reciprocity,

$$H_{z1212}(\phi, \phi_o) = D_{1212}(\phi, \phi_o)\,\frac{e^{-jk\rho}}{\sqrt{\rho}}e^{-jkw\,\sin\phi_o} = H_{z2121}(\phi_o, \phi) = D_{2121}(\phi_o, \phi)\,\frac{e^{-jk\rho}}{\sqrt{\rho}}e^{-jkw\,\sin\phi_0} \tag{39}$$

where $D_{1212}(\phi, \phi_0) = D_{2121}(\phi_0, \phi)$ is the diffraction coefficient associated with the quadruply diffracted field.

VII. QUINTUPLY DIFFRACTED FIELDS

The mechanisms associated with fifth order diffraction are illustrated in Figure 7.

Proceeding as before, the quintuply diffracted field $H_{z12121}(\phi, \phi_o)$ can be expressed as

$$H_{z12121}(\phi,\phi_o)=\Delta\int_{S(0)}\left[\sec\left(\frac{\alpha-3\pi/2+\phi_o}{2}\right)+\sec\left(\frac{\alpha-3\pi/2-\phi_o}{2}\right)\right]\left(-\frac{e^{-j\pi/4}}{2\sqrt{2\pi k}}\right)$$

$$\left[H_z^e\left(\alpha+\frac{\pi}{2},\phi_o\right)-H_z^m\left(\alpha+\frac{\pi}{2},\phi_o\right)\right]D_{1212}\left(\phi,\frac{\pi}{2}+\alpha\right)e^{-jkw\cos\alpha}\,d\alpha \qquad (40)$$

in which $D_{1212}(\phi, \pi/2+\alpha)$ is defined in (36)-(38), but must be modified in view of (29). We have

$$D_{1212}\left(\phi,\frac{\pi}{2}+\alpha\right)=\Bigg\{-\sqrt{2\pi kw}\;e^{j\pi/4}\left[I\left(\frac{3\pi}{2}-\phi,0\right)+I\left(\frac{3\pi}{2}+\phi,0\right)\right]\left[I(-\pi-\alpha,0)+I(\alpha,0)\right]$$

$$+j2\pi kw\left\{-\sqrt{2\pi kw}\;e^{j\pi/4}\left[\sec\left(\frac{3\pi/2-\phi-\alpha}{2}\right)+\sec\left(\frac{3\pi/2+\phi-\alpha}{2}\right)\right]+I\left(\alpha,\frac{3\pi}{2}-\phi\right)+I\left(\alpha,\frac{3\pi}{2}+\phi\right)\right\}$$

$$+\left\{-\sqrt{2\pi kw}\;e^{j\pi/4}\left[I_1\left(\frac{3\pi}{2}-\phi\right)+I_1\left(\frac{3\pi}{2}+\phi\right)\right]+I(0,0)\left[I\left(\frac{3\pi}{2}-\phi,0\right)+I\left(\frac{3\pi}{2}+\phi,0\right)\right]\right\}$$

$$\bullet\left[I(-\pi-\alpha,0)+I(\alpha,0)\right]\Bigg\}\left(\frac{e^{-jkw}}{\sqrt{w}}\right)^3F_4\left(0,\frac{\pi}{2}+\alpha,\phi\right) \qquad (41)$$

for $\alpha\approx 0$. Performing now a uniform evaluation of (40), as before, we obtain

$$H_{z12121}(\phi,\phi_o)=\Bigg\{-\sqrt{2\pi kw}\;e^{j\pi/4}\left[I_1\left(\frac{3\pi}{2}-\phi,0\right)+I_1\left(\frac{3\pi}{2}+\phi,0\right)\right]$$

$$\left\{-\sqrt{2\pi kw}\;e^{j\pi/4}\left[I_1\left(\frac{3\pi}{2}-\phi_o\right)+I_1\left(\frac{3\pi}{2}+\phi_o\right)\right]+I(0,0)\left[I\left(0,\frac{3\pi}{2}-\phi_o\right)+I\left(0,\frac{3\pi}{2}+\phi_o\right)\right]\right\}$$

$$+j2\pi kw\left\{-\sqrt{2\pi kw}\;e^{j\pi/4}\left[I\left(\frac{3\pi}{2}-\phi,\frac{3\pi}{2}-\phi_o\right)+I\left(\frac{3\pi}{2}-\phi,\frac{3\pi}{2}+\phi_o\right)+I\left(\frac{3\pi}{2}+\phi,\frac{3\pi}{2}-\phi_o\right)\right.\right.$$

$$\left.\left.+I\left(\frac{3\pi}{2}+\phi,\frac{3\pi}{2}+\phi_o\right)\right]+\left[I\left(0,\frac{3\pi}{2}-\phi\right)+I\left(0,\frac{3\pi}{2}-\phi\right)\right]\left[I\left(0,\frac{3\pi}{2}-\phi_o\right)+I\left(0,\frac{3\pi}{2}-\phi_o\right)\right]\right\}$$

$$+\left\{-\sqrt{2\pi kw}\, e^{j\pi/4}\left[I_1\left(\frac{3\pi}{2}-\phi\right)+I_1\left(\frac{3\pi}{2}+\phi\right)\right]+I(0,0)\left[I\left(\frac{3\pi}{2}-\phi,0\right)+I\left(\frac{3\pi}{2}+\phi,0\right)\right]\right\}$$

$$\cdot\left\{-\sqrt{2\pi kw}\, e^{j\pi/4}\left[I_1\left(\frac{3\pi}{2}-\phi_o\right)+I_1\left(\frac{3\pi}{2}+\phi_o\right)\right]+I(0,0)\left[I\left(0,\frac{3\pi}{2}-\phi_o\right)+I\left(0,\frac{3\pi}{2}+\phi_o\right)\right]\right\}\Bigg\}$$

$$\cdot F_5\left(0,\phi,\phi_o\right)\left(\frac{e^{-jkw}}{\sqrt{w}}\right)^4 \frac{e^{-jk\rho}}{\sqrt{\rho}} = D_{12121}\left(\phi,\phi_o\right)\frac{e^{-jk\rho}}{\sqrt{\rho}} \tag{42}$$

in which

$$F_5\,(0,\phi,\phi_o) = -\frac{e^{-j\pi/4}}{2\sqrt{2\pi k}}\left[H_z^e\left(\frac{\pi}{2},\phi_o\right)-H_z^m\left(\frac{\pi}{2},\phi_o\right)\right]F_4\left(0,\frac{\pi}{2},\phi\right) \tag{43}$$

where $F_4(0, \phi, \phi_0)$ is defined in (38). The evaluation of the diffraction coefficient $D_{21212}\ (\phi, \phi_0)$ can be deduced from $D_{12121}\ (\phi, \phi_0)$ by interchanging ϕ and ϕ_0 in (42) and by replacing $F_5\ (0, \phi, \phi_0)$ with

$$F_5'\ (0,\phi,\phi_0) = -\frac{e^{-j\pi/4}}{2\sqrt{2\pi k}}\,\eta_{1R}\,K_+\left(\frac{\pi}{2},\eta_{1R}\right)K_+\left(\phi_0,\eta_{1R}\right)F_4\left(0,\phi,\frac{\pi}{2}\right). \tag{44}$$

IIX. NUMERICAL RESULTS

To test the validity of the derived diffraction coefficients it is instructive to first consider the special case when both half planes are perfectly conducting. The derived diffracted fields are then valid everywhere (unless shadowed) and this should, therefore, allow verification of the continuity of the scattered field which is equal to the sum of the diffracted fields. Every diffraction mechanism has a shadow boundary either at $\phi = \pi/2$ or $\phi = 3\pi/2$; however, the total field should remain continuous because of appropriate sign reversals in the unshadowed diffracted fields. For example, given that $\pi/2 < \phi_0 < 3\pi/2$, H_{z2} is shadowed in the region $0 < \phi < \pi/2$ and thus discontinuous at $\phi = \pi/2$. However, at $\phi = \pi/2$ the terms of H_{z12} associated with a transition function whose argument vanishes at this boundary, experience a reversal of their sign so that the sum $H_{z2} + H_{z12}$ remains continuous at $\phi = \pi/2$. Similarly $H_{z21} + H_{z121}$, $H_{z212} + H_{z1212}$ and $H_{z2121} + H_{z12121}$ are continuous at $\phi = \pi/2$.

Shown in Fig. 8 are backscatter and bistatic patterns for two parallel perfectly conducting half planes separated by a distance $w = 1.55\ \lambda$. It is seen that the high frequency solution is in good agreement with the exact [11] pattern. We also observe that the primary role of the multiply diffracted fields beyond the second order is to maintain continuity of the scattered field at the shadow boundaries $\phi = \pi/2$ and $\phi = 3\pi/2$. As noted earlier, of interest in this study was to examine whether the derived high frequency solution remained valid when w was much less than a wavelength. The pattern in Fig. 9 corresponds to the case when $w = 0.05\ \lambda$ and it is clear that the derived high frequency solution is still in good agreement with the exact.

For the general case when the half planes satisfy the boundary conditions (2) and (4), there is no available exact solution, neither is it possible to generate numerical data of acceptable accuracy. However, when R=0 and w is small, the pair of half sheets represent a metal backed dielectric half plane which is traditionally modelled as an impedance half plane [12]. Also, recently [13], an improved solution was obtained using a second order boundary condition to simulate the coated surface of the half plane. Data based on these formulations can then be employed in examining the validity of the presented high frequency solution. Figure 10 presents backscatter patterns for a coated half plane as computed by this high frequency solution and those based on the standard [12] and second order [13] impedance boundary conditions. It is again observed that the high frequency solution derived here is in general agreement with that predicted by using a second order boundary condition to simulate the coating. This was, of course, to be expected because like the second order boundary condition given in (2), the formulation in [13] also allows a simulation of the normal polarization currents within the dielectric. In contrast, the standard impedance boundary condition (a first order condition) lacks such a capability and does not provide an accurate simulation near edge-on incidences. It should be noted, though, that since the solution given in [13] is also approximate, its small disagreement with that predicted by the two sheet simulation is not necessarily indicative of the accuracy of that solution.

Echowidth patterns corresponding to the case when $R \neq 0$ are shown in Fig. 11. One characteristic of these backscatter patterns is their independence on the value of R at edge-on incidence. This is particularly true for H polarization, where the resistive half plane is much less observable in that region. As a result, the entire scattering contribution is primarily caused by the dielectric half-plane itself.

IX. SUMMARY

In this report, the extended spectral ray method (ESRM) was employed to derive the multiply diffracted fields for a pair of semi-infinite parallel sheets (material layers). The top sheet was chosen to satisfy a second order boundary condition simulating a thin dielectric layer and the lower one was a resistive sheet. Of interest was the computation of the leading edge scattering given by the sum of the singly and multiply diffracted fields. Particular attention was given on the computation of the higher order fields beyond the second since their derivation required a deviation from the traditional ESRM. This was because the diffracted fields beyond the second order were associated with ray paths traversing along reflection boundaries. The resulting spectral representation of these fields then consisted of highly oscillatory components which were essentially decomposed into a pair of slowly varying ones before evaluation of the spectral integrals.

Up to fifth order diffracted fields were derived and employed in scattering computations demonstrating their validity. For a pair of perfectly conducting half planes, the generated echowidth patterns were shown to agree with exact data for separation distances as small as one tenth of a wavelength. Comparisons were also provided with other solutions simulating a metal-backed dielectric half plane with favorable agreements.

In closing, it should be noted that the given solution can be easily modified for the case when the resistive half plane is replaced by a thin dielectric layer similar to the other. Once this is accomplished, a solution for E polarization can be obtained by invoking duality.

REFERENCES

1. T.B.A. Senior and J.L. Volakis, "Sheet Simulation of a Thin Dielectric Layer," Radio Sci., vol. 22, 1261-1272, 1987.

2. L.A. Weinstein, *The theory of diffraction and factorization method*, Golem Press: Boulder, CO, 1969, p. 301.

3. T.B.A. Senior, "Combined Resistive and Conductive Sheets," IEEE Trans. Antennas Propagat., vol. AP-33, pp. 577-579, 1985.

4. R. Tiberio and R.G. Kouyoumjian, "A Uniform GTD Solution for the Diffraction by Strips at Grazing Incidence," Radio Sci., vol. 14, pp. 933-941, 1979.

5. M.I. Herman and J.L. Volakis, "High Frequency Scattering by a Resistive Strip and Extensions to Conductive and Impedance Strips," Radio Sci., vol. 22, pp. 335-349, May-June 1987.

6. M.I. Herman and J.L. Volakis, "High Frequency Scattering by a Double Impedance Wedge," IEEE Trans. Antennas Propagat., vol. AP-36, pp. 664-678, May 1988.

7. J.L. Volakis, "High Frequency Scattering by a Thin Material Half Plane and Strip," Radio Sci., vol. 23, pp. 450-462, May-June 1988.

8. J.L. Volakis and T.B.A. Senior, "Simple Expressions for a Function Occurring in Diffraction Theory," IEEE Trans. Antennas & Propagat., vol. AP-33, pp. 678-680, 1985.

9. R.G. Kouyoumjian and P.H. Pathak, " A Uniform Geometrical Theory of Diffraction for an Edge in a Perfectly Conducting Surface," Proc. IEEE, vol. 62, pp. 1448-1461, 1974.

10. H.H. Syed and J.L. Volakis, "Multiple Diffractions Among Polygonal Impedance Cylinders," IEEE Trans Antennas & Propagat., May 1989.

11. J.L. Volakis and M.A. Ricoy, "Diffraction by a Thick Perfectly Conducting Half Plane," IEEE Trans. Antennas and Propagat., vol. AP-34, pp. 172-180, Feb. 1986.

12. G.D. Maliuzhinets, "Excitation, Reflection and Emission of Surface Waves from a Wedge with Given Face Impedances," Sov. Phys. Dokl., Engl. Transl., Vol. 3, pp. 752-755, 1958.

13. J.L. Volakis and T.B.A. Senior, "Application of a Class of Generalized Boundary Conditions to Scattering by a Metal-Backed Dielectric Half Plane," Proc. IEEE, May 1989.

List of Figures

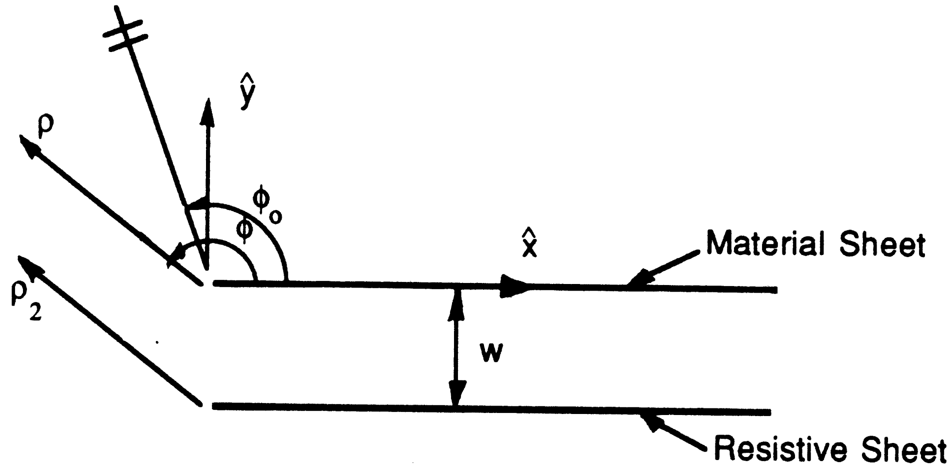

Fig. 1. Geometry of the resistive and material half sheets.

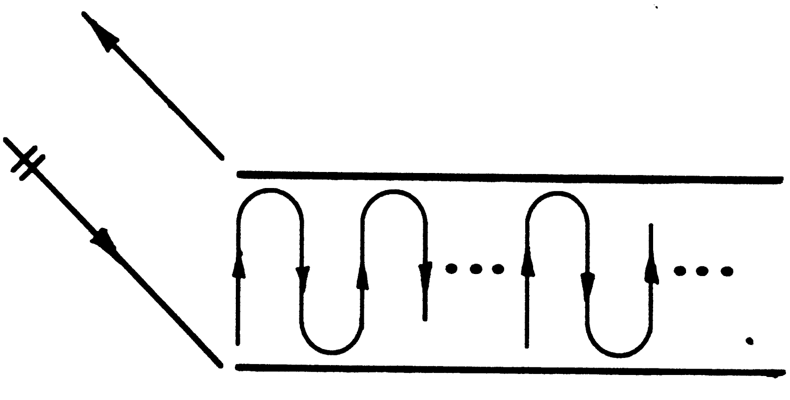

Fig. 2. Illustration of propagation along reflection boundaries for higher order mechanisms beyond the second.

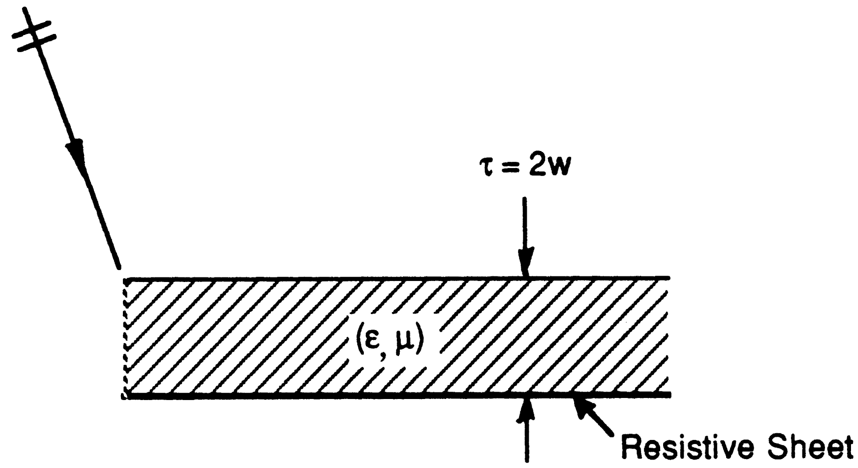

Fig. 3. Geometry of a thin semi-infinite dielectric layer backed by a resistive half sheet. Provided $\tau \leq 0.1\,\lambda$, this configuration can be simulated by the pair of half sheets in fig. 1 with $\tau = 2w$.

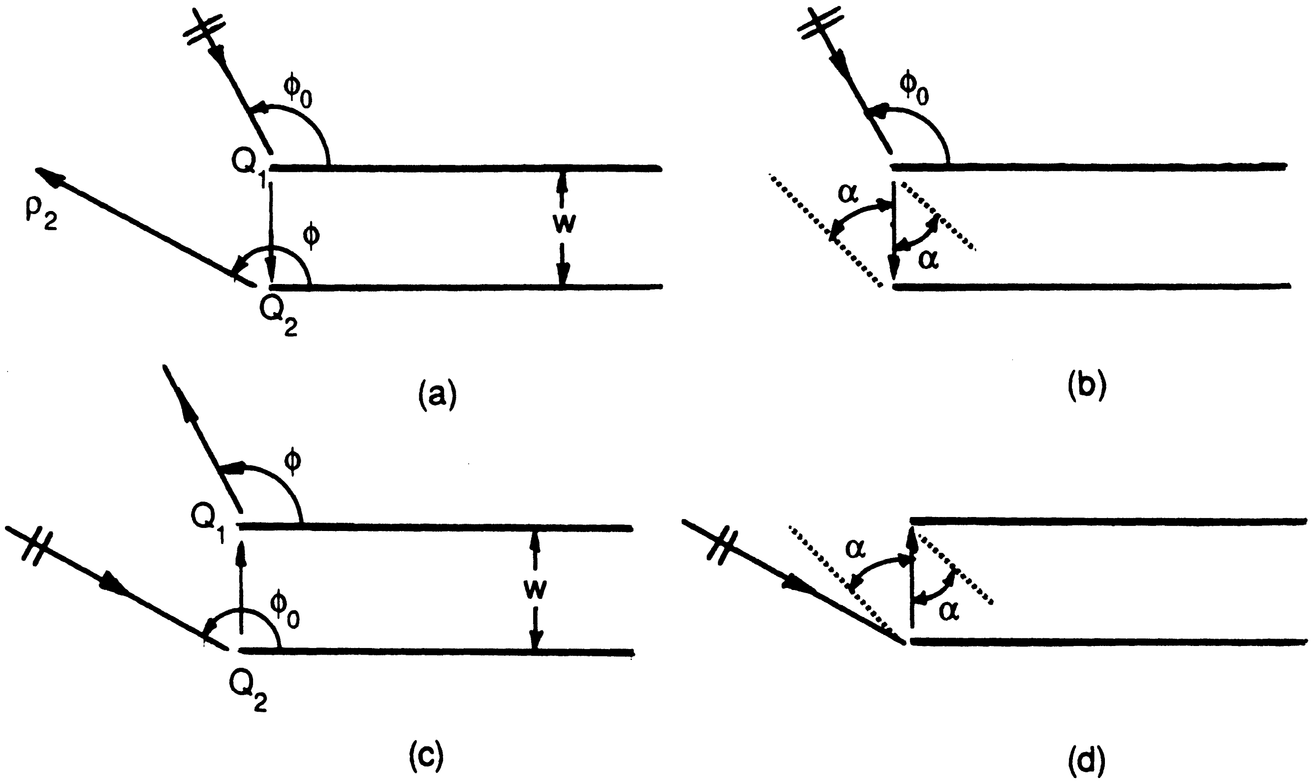

Fig. 4. Illustration of the double diffraction mechanisms.

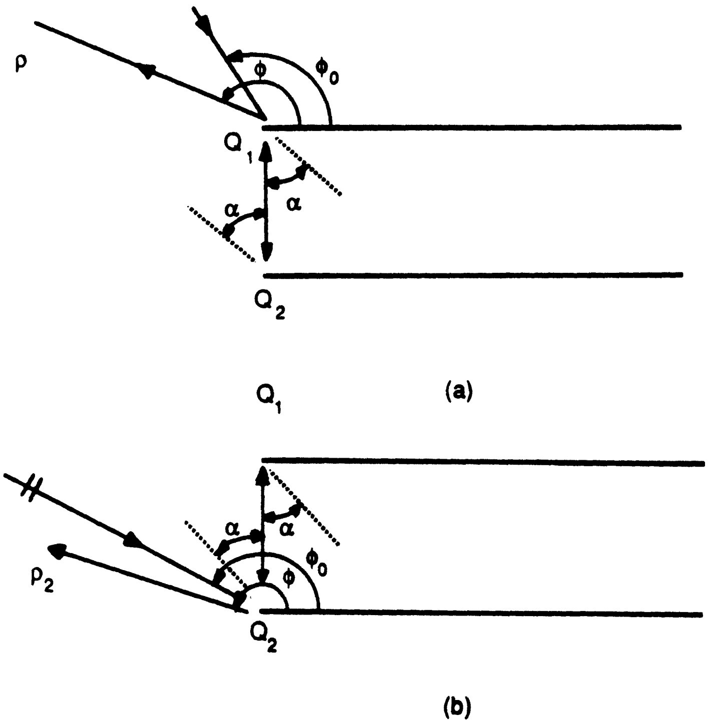

Fig. 5. Illustration of the triple diffraction mechanism.

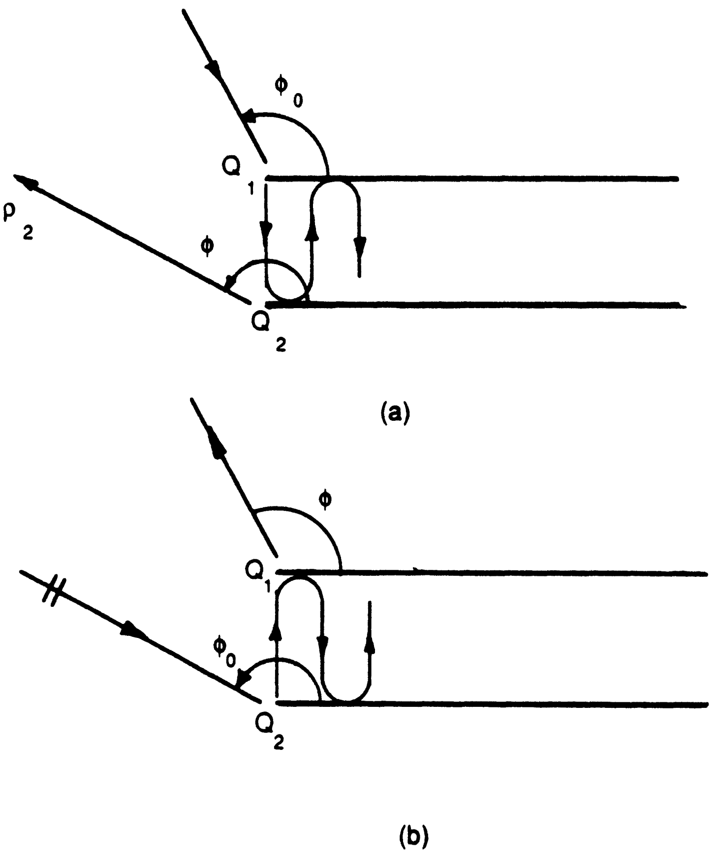

Fig. 6. Illustration of the fourth order diffraction mechanisms.

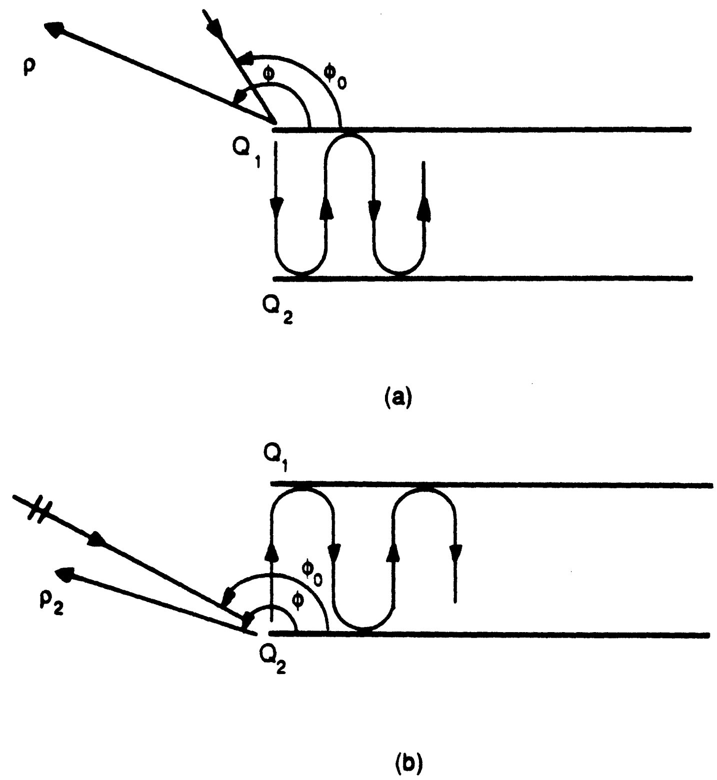

Fig. 7. Illustration of the fifth order diffraction mechanisms.

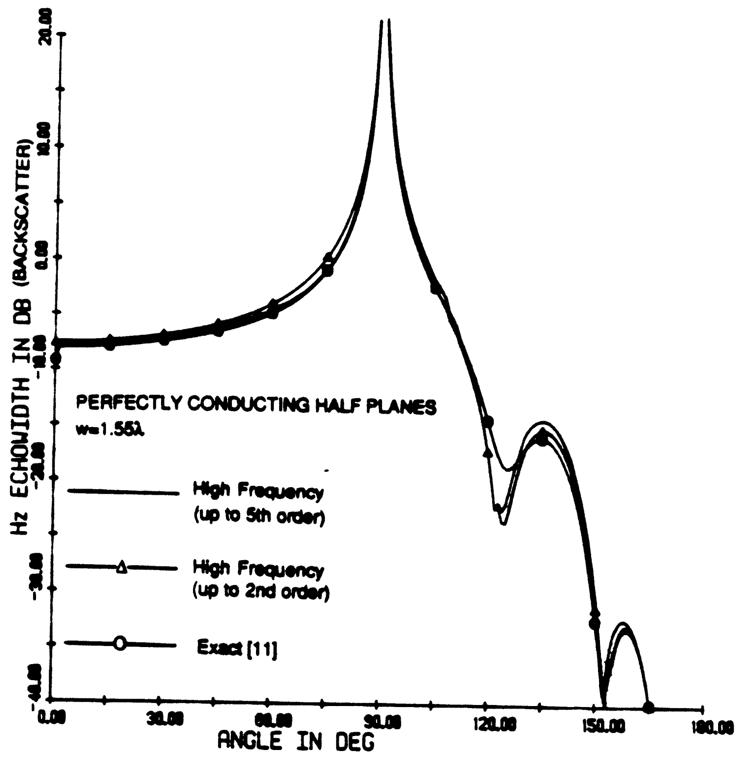

(a)

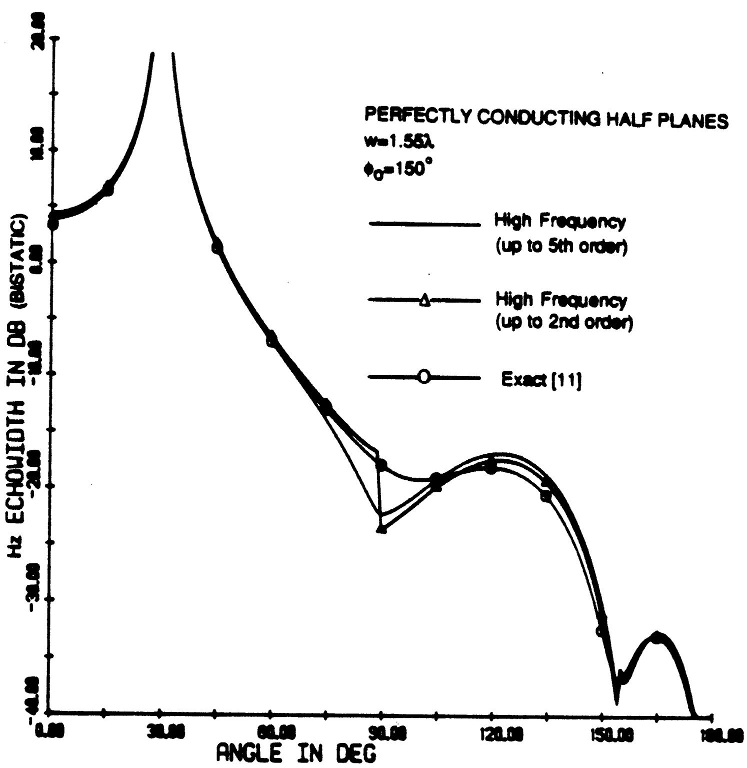

(b)

Fig. 8. H_z echowidth pattern for a pair of perfectly conducting parallel half planes seperated by 1.55 wavelengths; comparison of high frequency and exact patterns. (a) Backscatter. (b) Bistatic pattern; $\phi_0 = 150°$.

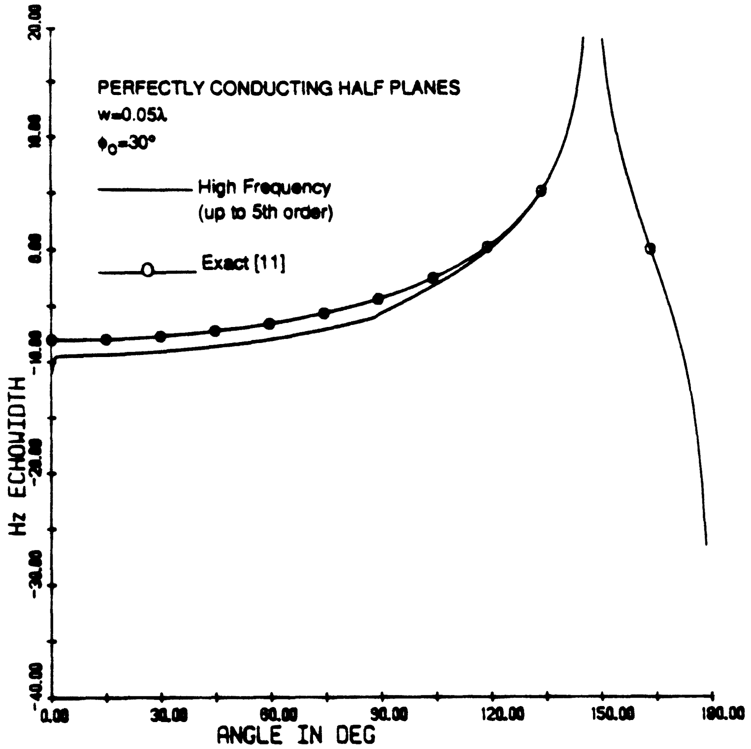

(a)

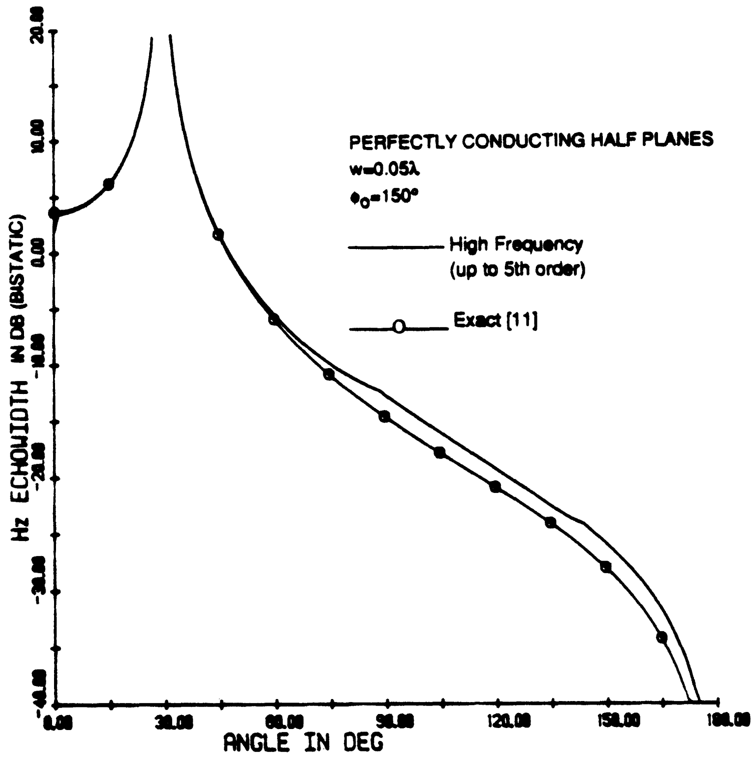

(b)

Fig. 9. Bistatic H_z echowidth pattern for a pair of perfectly conducting half planes separated by 1/20 of a wavelength; comparison of high frequency and exact data. (a) $\phi_0 = 30°$. (b) $\phi_0 = 150°$.

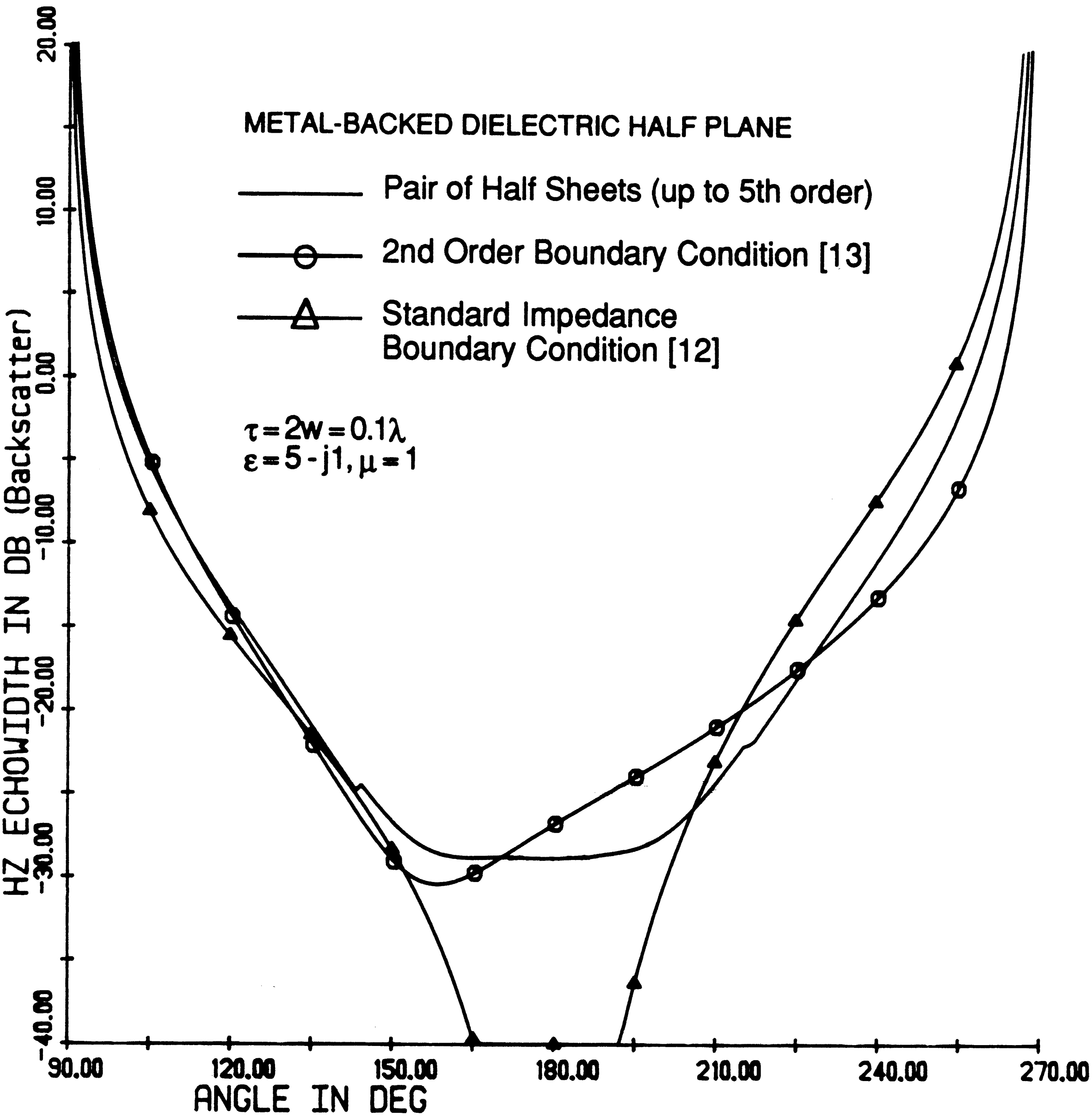

Fig. 10. Backscatter H_z echowidth pattern for a metal-backed dielectric half plane of thickness 0.1λ and having $\varepsilon=5-j1$; comparison of this solution with those based on simulations of the coating using the standard and a second order impedance boundary condition.

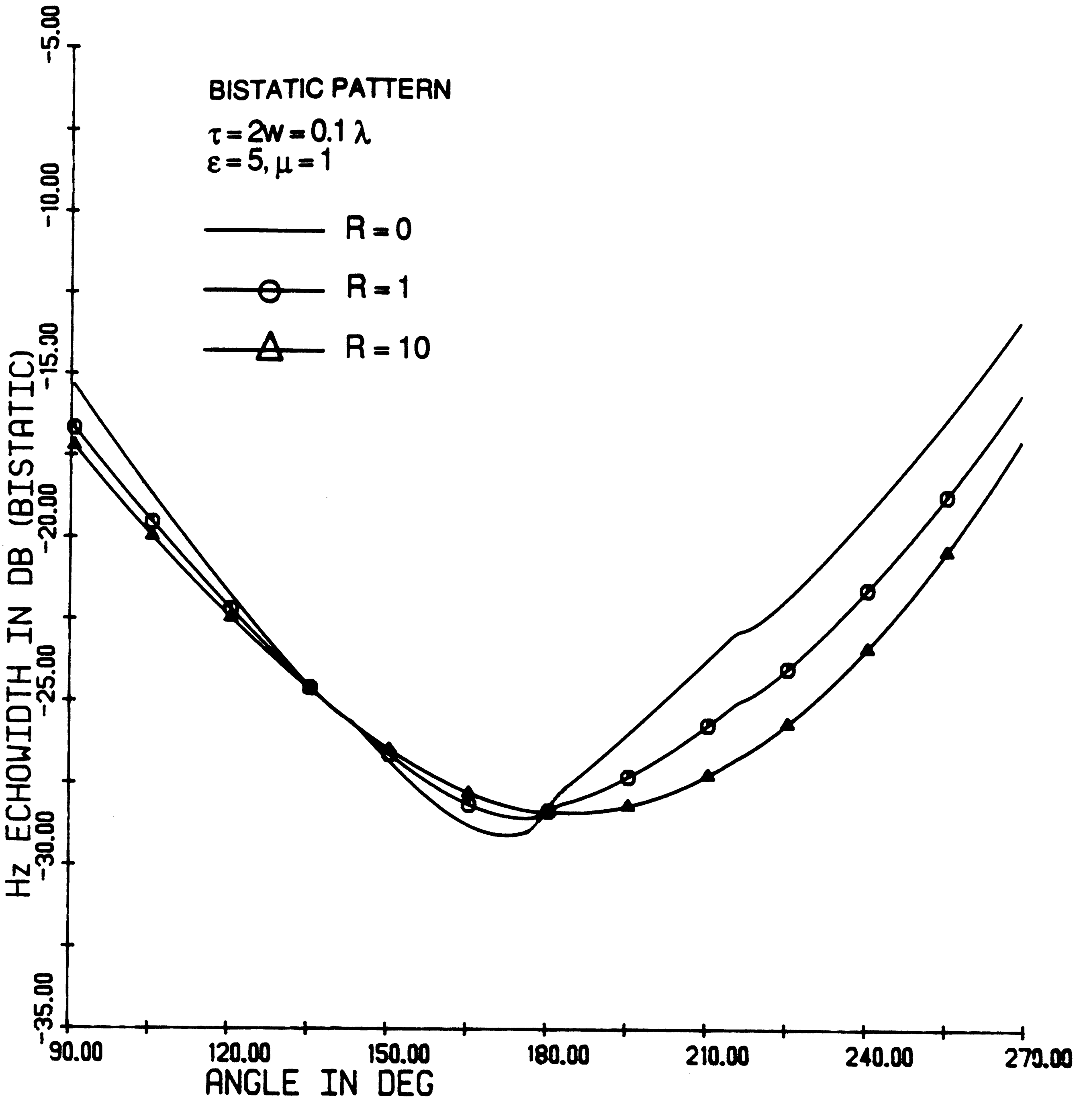

Fig. 11. **Bistatic Hz echowidth patterns for a dielectric half plane (ε=5, τ=2w=0.1λ) backed by a resistive half plane having resistivites R=0, 1 and 10.**

APPENDIX A

DERIVATION OF BOUNDARY CONDITIONS FOR A DIELECTRIC LAYER ON A RESISTIVE SHEET

Consider a dielectric/ferrite layer residing on a resistive sheet as shown in Figure 1A. Below our goal is to derive boundary conditions to effectively replace the composite effect of the dielectric/ferrite layer on the resistive sheet. Two approaches are considered in accomplishing this. One involves (approach A) transferring the effect of the dielectric/ferrite layer to the location of the resistive sheet. Another, shifts the resistive sheet condition to the center of the layer. In the following we derive the appropriate boundary conditions for H_z-incidence ($E_z = H_x = H_y = 0$) followed by a similar analysis for E_z-incidence ($H_z = E_x = E_y = 0$).

H-polarization - Approach A

Referring to Figure 1A, at y = 0 the boundary conditions due to the presence of the resistive sheet are

$$2RZ\,[H_z(0^+) - H_z(0^-)] = E_x(0^+) + E_x(0^-) = 2E_x(0^-)$$
$$E_x(0^+) = E_x(0^-) \qquad (1)$$

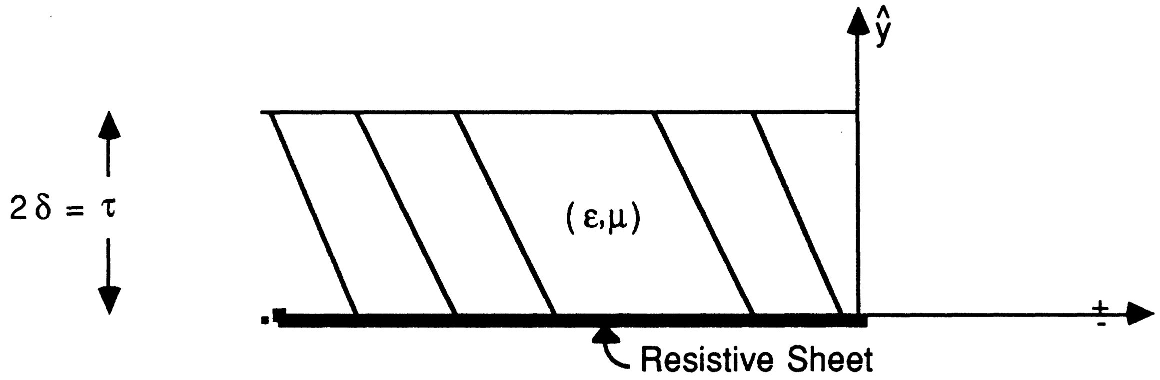

Fig. 1A. Geometry of a dielectric/ferrite layer on a resistive sheet for Approach A.

where R denotes the normalized sheet resistivity, Z is the free space intrinsic impedance and $H_z(0^{\pm})$ refers to the field value at $y = 0^{\pm}$ (that is, above or below the resistive sheet). To account for the presence of the dielectric/ferrite layer we may now expand $E_x(0^+)$ and $H_z(0^+)$ using the first two terms of a Taylor Series expansion giving

$$E_x(0^+) = E_x(2\delta^-) - 2\delta \frac{\partial E_x(2\delta^-)}{\partial y}$$

$$= E_x(2\delta^+) - \frac{2\delta}{\varepsilon}\frac{\partial E_y(2\delta^+)}{\partial x} + i\, 2\delta k\mu Z\, H_z(2\delta^+) \tag{2a}$$

$$H_z(0^+) = H_z(2\delta^-) - 2\delta \frac{\partial H_z(2\delta^-)}{\partial y} = H_z(2\delta^-) + i\,\frac{2\delta k\varepsilon}{Z} E_x(2\delta^+) \tag{2b}$$

in which ε and μ are the relative permittivity and permeability of the dielectric/ferrite layer, respectively, k denotes the free space wave number and an $e^{-i\omega t}$ convention has been assumed and suppressed.

Substituting (2) in (1) we obtain

$$R\,Z\left[H_z(2\delta^+) + \frac{i2\delta k\varepsilon}{Z} E_x(2\delta^+) - H_z(0^-)\right] = E_x(0^-)$$

$$E_x(0^-) = E_x(2\delta^+) - \frac{2\delta}{\varepsilon}\frac{\partial E_y(2\delta^+)}{\partial x} + i2\delta k\mu Z\, H_z(2\delta^+) \tag{3}$$

We may again transfer the fields back to $y = 0^+$ through another application of a Taylor Series expansion to find

$$H_z^+ - H_z^- = \frac{1}{RZ} E_x^- + \frac{2}{\eta_e Z} E_x^+$$

$$E_x^+ - E_x^- = +\frac{2}{ik\eta_e^*}\frac{\partial E_x^+}{\partial y} + \frac{2Z}{\eta_m^*} H_z^+ \tag{4}$$

with

$$\eta_e^* = \frac{2i\varepsilon}{2k\delta\,(\varepsilon-1)} \qquad \eta_m^* = \frac{2i}{2k\delta\,(\mu-1)}\ , \qquad \eta_e = \frac{2i}{2k\delta\,(\varepsilon-1)} \tag{5}$$

and we have set $H_z^\pm = H_z(0^\pm)$. Similarly $E_x^\pm = E_x(0^\pm)$.

The boundary conditions (4) are applied at y = 0 and represent an approximate replacement of the configuration in Figure 1A. However, they can be shown to be most accurate for small R. In addition, their derivation implies that δ is small with respect to the wavelength within the dielectric/ferrite layer. Obviously, they represent co-planar electric and magnetic sheet currents, but unlike previously encountered ones, these are now coupled, except when R = 0. In this case the electric currents vanish and (4) reduce to those given earlier.

E-polarization - Approach A

Referring again to Figure 1A, the boundary condition with E_z-incidence at y = 0 due to the presence of the resistive sheet are

$$-RZ\left[H_x(0^+) - H_x(0^-)\right] = E_z(0^-)$$

$$E_z(0^+) = E_z(0^-) \tag{6}$$

As before, to account for the presence of the dielectric/ferrite layer we expand $H_x(0^+)$ and $E_z(0^+)$ using the first two terms of the Taylor Series expansion to obtain

$$-RZ\left[H_x(2\delta^+) - \frac{2\delta}{\mu}\frac{\partial H_y(2\delta^+)}{\partial x} - \frac{i2\delta k\varepsilon}{Z}E_z(2\delta^+) - H_x(0^-)\right] = E_z(0^-) \tag{7}$$

$$E_z(0^-) = E_z(2\delta^+) - i2\delta kZ\mu\, H_x(2\delta^+)$$

Transferring now the fields from y = $2\delta^+$ back to y = 0^+, we finally obtain

$$H_x^+ - H_x^- = -\frac{E_z^-}{RZ} + \frac{2}{ik\eta_m}\frac{\partial H_y^+}{\partial x} - \frac{2}{\eta_e Z}E_z^+ \tag{8}$$

$$E_z^+ - E_z^- = -\frac{2Z}{\eta_m^*}H_x^+$$

with

$$\eta_m = \frac{2i\mu}{2k\delta\,(\mu-1)} \quad . \tag{9}$$

Similarly to the H-polarization case, (8) is best for small R and results to coupled integral equations for the determination of the electric and magnetic currents defined as

$$H_x^+ - H_x^- = -J_z$$

$$E_z^+ - E_z^- = -M_x \tag{10}$$

H-polarization - Approach B

Under this approach the resistive sheet boundary condition is transferred to the center of the layer to be combined with the equivalent sheets of the dielectric/ferrite layer. It is, therefore, convenient to reposition the coordinate system to have its origin at the center of the dielectric/ferrite layer as shown in Figure 2A.

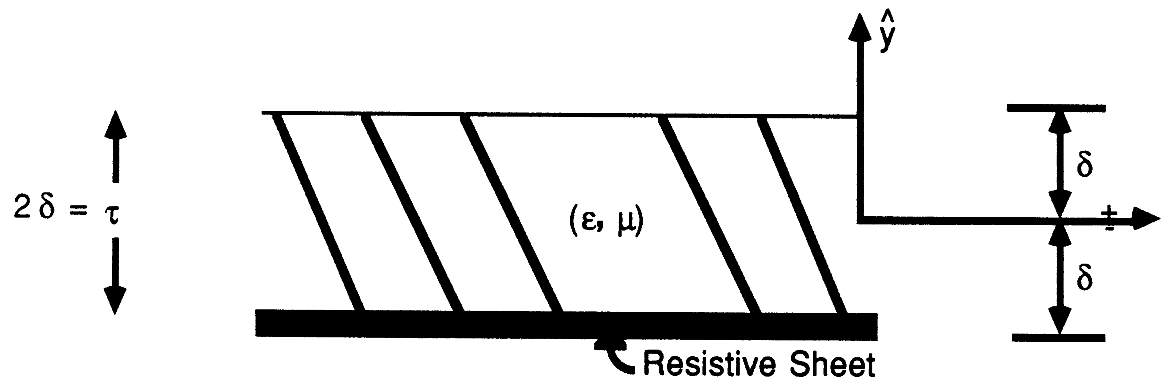

Fig. 2A. Geometry of a dielectric/ferrite layer on a resistive sheet for Approach B.

Referring to this new coordinate system, let us now assume that the field at y = 0 is E_x^m and attempt to bring in the effect of the material in the regions y > 0 and y < 0 by employing the usual two term Taylor Series expansion. We obtain

$$E_x^m = E_x(\delta^-) - \delta \frac{\partial E_x(\delta^-)}{\partial y} = E_x(\delta^-) - \delta \left[\frac{\partial E_y(\delta^-)}{\partial x} - ik\mu_r ZH_z(\delta^-) \right] \tag{11}$$

and by invoking the boundary conditions relating the fields at $y = \delta^+$ and $y = \delta^-$ we have

$$E_x^m = E_x(\delta^+) - \delta\left[\frac{1}{\varepsilon}\frac{\partial E_y(\delta^+)}{\partial x} - ik\mu\; ZH_z(\delta^+)\right] \tag{12}$$

Transferring now the fields at y = 2δ⁺ back to y = 0⁺ we obtain

$$E_x^m = E_x^+ - \delta\left[\left(\frac{1}{\varepsilon} - 1\right)\frac{\partial E_y^+}{\partial x} - ik\,(\mu-1)\,Z\,H_z^+\right] \tag{13}$$

where, as usual, we have set $H_z^+ = H_z\,(0^+)$ and $E_x^+ = E_x\,(0^+)$.

A similar expansion of the fields in the region y < 0 yields

$$E_x^m = E_x(-\delta^+) + \delta\,\frac{\partial E_x(-\delta^+)}{\partial y} = E_x(-\delta^-) + \delta\left[\frac{1}{\varepsilon}\frac{\partial E_y(-\delta^-)}{\partial x} - ik\mu\,Z\,H_z(-\delta)\right] \tag{14}$$

where consistent with the previous notation $E_x\,(-\delta^+)$ denotes the field's value at y = -δ just inside the dielectric and, of course, above the resistive sheet. Similarly, $E_x\,(-\delta^-)$ denotes the field's value outside the dielectric's surface at y = -δ and above the resistive sheet. To account for the presence of the resistive sheet we now recall the resistive sheet boundary conditions

$$2R\left[H_z(-\delta^-) - H_z(-\delta^=)\right] = E_x(-\delta^-) + E_x(-\delta^=) = 2\,E_x(-\delta^-)$$

$$E_x(-\delta^-) = E_x(-\delta^=) \tag{15}$$

where $E_x\,(-\delta^=)$ implies the field's value on the lower side of the resistive sheet. Thus, on the assumption that R ≠ 0 we have

$$H_z(-\delta^-) = H_z(-\delta^=) + \frac{E_x(-\delta^=)}{R}$$

$$E_x(-\delta^-) = E_x(-\delta^=) \tag{16}$$

and the first of these also implies

$$E_y(-\delta^-) = E_y(-\delta^=) + \frac{Z}{ikR}\frac{\partial E_y(-\delta^=)}{\partial x} \tag{17}$$

Since

$$E_y = -\frac{iZ}{k}\frac{\partial H_z}{\partial x}$$

Substituting (16) - (17) into (14) we now obtain

$$E_x^m = E_x(-\delta^=) + \delta\left[\frac{1}{\varepsilon}\frac{\partial E_y(-\delta^=)}{\partial x} + \frac{1}{ik\varepsilon R}\frac{\partial^2 E_x(-\delta^=)}{\partial x^2} - ik\mu Z\,H_z(-\delta^=) - ik\mu Z\frac{E_x(-\delta^=)}{R}\right] \tag{18}$$

and by transferring the fields back to y = 0⁻, (18) becomes

$$E_x^m = E_x^- + \frac{1}{ik\eta_e^*}\frac{\partial E_y^-}{\partial x} + \frac{1}{\eta_m^*}ZH_z^- + \frac{\delta}{ik\varepsilon R}\frac{\partial^2 E_x^-}{\partial x^2} - ik\mu\delta Z\frac{E_x^-}{R} \tag{19}$$

valid to 0(δ). Equations (13) and (19) now represent two expressions for E_x^m each involving components of the fields above or below y = 0. Eliminating E_x^m yields the boundary condition

$$E_x^+ - E_x^- = \frac{1}{ik\eta_e^*}\frac{\partial}{\partial x}(E_y^+ + E_y^-) + \frac{Z}{\eta_m^*}(H_z^+ + H_z^-) + \frac{\delta Z}{ik\varepsilon R}\frac{\partial^2 E_x^-}{\partial x^2} - \frac{ik\mu\delta Z}{R}E_x^- \tag{20}$$

Following a similar procedure we may now expand H_z in the y → 0 region of the layer to obtain

$$H_z^m = H_z^+ - \frac{1}{ik\eta_m}\frac{\partial H_y^+}{\partial z} - \frac{E_x^+}{\eta_e Z} = H_z^+ - \frac{E_x^+}{\eta_e Z} \tag{21}$$

where H_z^m is the field's value at y = 0. Also,

$$H_z^m = H_z(-\delta^-) - \frac{ik\varepsilon\delta}{Z}E_x(-\delta^-) \tag{22}$$

and again we may invoke the resistive sheet conditions (15) giving

$$H_z^m = H_z(-\delta^{=}) + \frac{E_x(-\delta^{=})}{R} - \frac{ik\varepsilon\delta}{Z} E_x(-\delta^{=}) \tag{23}$$

Transferring the fields in (23) back to y = 0^- and retaining terms to $0(\delta)$ yields

$$H_z^m = H_z(0^-) - \delta \frac{\partial H_z(0^-)}{\partial y} + \frac{E_x(0^-)}{R} - \frac{\delta}{R}\frac{\partial E_x(0^-)}{\partial y} - \frac{ik\delta\varepsilon}{Z} E_x(0^-)$$

$$= H_z^- + \frac{ik\delta}{Z} E_x^- + \frac{E_x^-}{R} - \frac{\delta}{R}\left[\frac{\partial E_y^-}{\partial x} - ikZ\, H_z^-\right] - \frac{ik\delta\varepsilon}{Z} E_x^-$$

or

$$H_z^m = H_z^- + \frac{E_x^-}{Z\eta_e} + \frac{E_x^-}{R} - \frac{\delta}{R}\frac{\partial E_x^-}{\partial y} \tag{24}$$

Equations (21) and (24) may now be combined to eliminate H_z^m giving

$$H_z^+ - H_z^- = \frac{1}{Z\eta_e}(E_x^+ + E_x^-) + \frac{1}{R}\left(E_x^- - \delta \frac{\partial E_x^-}{\partial y}\right) \tag{25}$$

The above boundary condition along with (20) form a complete set for the simulation of a layer backed by a resistive sheet. As noted earlier they are valid for $R \neq 0$ and we also observe that for $R \to \infty$ they reduce to the known boundary conditions for the isolated dielectric/ferrite layer [1, 2].

Clearly, (20) and (25) represent a co-planar pair of magnetic and electric current sheets. Unfortunately, they result into coupled integral equations for the solution of the sheet currents. So far, our attempts to decouple them have not been fruitful precluding us from obtaining an exact solution of the relevant half plane problems. An alternative, though, is to consider a simulation of the geometry using a pair of parallel sheets (see fig. 3) whose solutions in isolation are known. Referring to Fig. 1A, the obvious choice is a resistive sheet at y=0, and another sheet (supporting electric and magnetic currents) placed at y=$\tau/2$ to simulate the dielectric layer. The boundary condition associated with the last has been derived in [1]. A high frequency solution of the diffraction by a pair of such sheets is now possible and in view of previous experience, it is expected that the inclusion of a sufficient number of higher order diffraction effects should allow an accurate characterization of their scattering.

APPENDIX B

COMPUTER PROGRAM LISTING

```
C  DIELRHP: Program for computing the scattered field by a          C
C       a pair of half planes, one simulating a resistive           C
C       half sheet and the other a thin semi-infinite dilectric     C
C       layer.                                                      C
C       Includes up to fifth order diffraction terms                C
C     Compile with HZ1M,HZIR,DOUB21,TRIP1,TRIP2,QUAD,QUINT1,SEC     C
C     FFUN,FI,FIP,FI1,KPLUSM,PSIPI,HEE,CSQRC,BTAN2,FFCT,GENPLO      C
C                                                                   C
      COMPLEX ER,UR,CJ4,CJ,DENOM1,DENOM2,RES,RSTAR,RSTARE,RSTARM
      COMPLEX ETAE,ETAMS,ETAES,ETAS,ETA1,TEMPC,ETAM1,ETAM2,ETAR
      COMPLEX KPLUSC,CON1,CON2,KPLUSM,TEMP1,TEMP2,RU,RL
      COMPLEX HZ1,HZ2,HZ21,HZ12,HZ121,HZ212,HZ412,HZ421,HZ51,HZ52
      COMPLEX TH1,TH1S,TH2S,HEE,THO,THN,THR,AA,BB,CC,RR,TT,RR1,TT1
      COMPLEX DOUB,TRIP,DUBM,TRIPMG,PHASI,PHASS,DUBE,TRIPE
      COMPLEX TT1I,TT1S,TTI,TTS
      DIMENSION ANG(361),HE(361),HM(361),HZ(361)
      DIMENSION HZF(361),HZS(361),HZT(361)
      COMMON /BLK1/ETA1,ETAR,ETAS,ETAES,ETAMS,ETAM1,ETAM2,CON1,CON2
      COMMON /BLK2/CJ,CJ4,PI,PI2
      COMMON /REFL/RU,RL,TT,TT1,PHASS,PHASI
      COMMON /THETAM/TH1,THR,TH1S,TH2S
      COMMON /THETAS/THO,THN
      PI=3.141592
      PI2=PI/2.
      CJ=(0.,1.)
      CJ4=CEXP(-CJ*PI/4.)
      PRINT *, 'NUMBER OF PLOTS,IPRINT,#OF RAYS:'
      READ(5,*) NPLOT,IPRINT,M,M2
      DO 2000 IPLOT=1,NPLOT
      PRINT *,'LAYER REL. PERMITT.,PERMEAB. AND THICKNESS(WL)'
      READ(5,*) ER,UR,THICK
      PRINT *,'IS THIS SIMULATING A THIN DIEL.H.P. ON A RES SHEET?'
      READ(5,*) ISIM
      IF(ISIM.NE.1) THEN
       PRINT *,'SEPARATION BETWEEN THE DIEL. AND RES. H.P.s:'
       READ(5,*) D
      ELSE
       D=THICK/2.
      ENDIF
      PRINT *,'NORM. RESISTIVITY OF THE RES. HALF PLANE:'
      READ(5,*) RES
      ETAR=1./(2.*RES)
      PRINT *,'ETAR:',ETAR
C ENSURE RIGHT BRANCH FOR LATER SQUARE ROOTS
      ER=ER-CJ*1.E-6
      UR=UR-CJ*1.E-6
      DENOM1=(ER-1)*2.*PI*THICK
      DENOM2=(UR-1.)*2.*PI*THICK
C COMPUTE ETA/IMPEDANCE PARAMETERS FOR USE IN DIFFR. COEFFICIENTS
      RES=-CJ/DENOM1
      RSTAR=-CJ/DENOM2
      RSTARE=-CJ*ER/DENOM1
      IF(CABS(ER).GT.1000.) THEN
       RSTARE=-CJ*ER/(2.*PI*(ER-1.)*.001)
      ENDIF
      RSTARM=-CJ*UR/DENOM2
      ETAE=2.*RES
      ETAMS=2.*RSTAR
      ETAES=2.*RSTARE
      ETAS=ETAES*ETAMS/(ETAES+ETAMS)
```

```
      ETA1=1./ETAE
C     PRINT *,'ETAES,PHAS:',ETAES,BTAN2(AIMAG(ETAES),REAL(ETAES))
      TEMPC=ETAS*ETAES
C     PRINT *,'ETES*ETAES,PHAS:',TEMPC,BTAN2(AIMAG(TEMPC),REAL(TEMPC))
      CON1=ETAS*CSQRT(1.+(4./TEMPC))
      PRINT *,'OLD TEMPC:',CON1
      TEMPC=ETAS*CSQRC(1.+(4./TEMPC))
C     PRINT *,'NEW TEMPC:',TEMPC
      ETAM1=.5*(ETAS+TEMPC)
      ETAM2=.5*(ETAS-TEMPC)
      TEMPC=KPLUSM((.5,0.),ETAM2,0,1.)/SIN(.25)
      PRINT *,'ETAES,ETAMS,ETAS:,',ETAES,ETAMS,ETAS
C     PRINT *,'ETAE,ETAM1,ETAM2:',ETAE,ETAM1,ETAM2,-1./ETAM1
      PRINT *,'INITIAL INCIDENCE AND SCATTERING ANGLES(DEG):'
      READ(5,*) PHI,PHS
      PHI=PHI*PI/180.
      PHS=PHS*PI/180.
      PRINT *,'INCREMENTS IN INCIDENT AND SCATTERING ANGLES,# OF PTS:'
      READ(5,*) DPHI,DPHS,NPTS
      DPHI=DPHI*PI/180.
      DPHS=DPHS*PI/180.
C      TH1=PI2-HEE(ETA1,0,1.)
C      THR=PI2-HEE(ETAR,0,1.)
C      TH1S=PI2-HEE(ETAM1,0,1.)
C      TH2S=PI2-HEE(ETAM2,0,1.)
CC     THO=PI2-HEE(ETAMS,0,1.)
C      THO=TH1
C      THN=THO
C       PRINT *,'THO,TH1S,TH2S:',THO,TH1S,TH2S
C       PRINT *,'CSIN(TH2S),1/ETAM2:',CSIN(TH2S),1./ETAM2
      DO 1000 I=1,NPTS
      CPHI=COS(PHI)
      CPHS=COS(PHS)
      SPHS=SIN(PHS)
      SPHI=SIN(PHI)
      CPHI2=COS(PHI/2.)
      CPHS2=COS(PHS/2.)
      SPHI2=SIN(PHI/2.)
      SPHS2=SIN(PHS/2.)
C Compute reflection and transmission coefficients
C   Incident ray refl & transm coef.
      AA=(1./ETAMS)+(CPHI*CPHI/ETAES)
      BB=SPHI
      CC=SPHI/ETAE
      RR=-(AA/(AA+BB))+(CC/(CC+1.))
      TTI=RR-((CC-1.)/(CC+1.))
      CC=SPHI*ETAR
      RR1=CC/(CC+1.)
      TT1I=1.-RR1
C  Scattered ray refl. & transm. coeff.
      AA=(1./ETAMS)+(CPHS*CPHS/ETAES)
      BB=SPHS
      CC=SPHS/ETAE
      RR=-(AA/(AA+BB))+(CC/(CC+1.))
      TTS=RR-((CC-1.)/(CC+1.))
      CC=SPHS*ETAR
      RR1=CC/(CC+1.)
      TT1S=1.-RR1
C NORMAL INCIDENCE REFL & TRANSM COEFFICIENTS
      RU=(1./(1.+ETAE))-(1./(1.+ETAMS))
```

```
      RL=ETAR/(1.+ETAR)
c      PRINT *,'CPHI,CPHS,SPHI2,SPHS2:',CPHI,CPHS,SPHI2,SPHS2
C      IF(CABS(ER).GT.1000.)THEN
       TT1=1-RL
       TT=1.-RU
C        TT1=(0.,0.)
C        TT=(0.,0.)
C      ENDIF
C        PRINT *,'RU,RL,TT,TT1',RU,RL,CABS(TTS),CABS(TTI)
C CALC FIRST ORDER DIFFRACTION
      CALL HZ1M(HZ1,PHI,PHS)
      PHASI=CEXP(-CJ*2.*PI*D*SPHI)
      PHASS=CEXP(-CJ*2.*PI*D*SPHS)
      CALL HZ1R(HZ2,PHI,PHS)
      HZ2=HZ2*CEXP(-CJ*2.*PI*D*(SPHI+SPHS))
C      PRINT *,'HZ2 SEC EDGE:',HZ2
C DOUBLE AND QUADRUPLE DIFFRACTION
      SGNS=1.
      SGNI=1.
      CALL DOUB21(HZ21,PHS,PHI,D,M,SGNS,SGNI)
      CALL QUAD(HZ421,PHS,PHI,D,1,SGNS,SGNI)
      HZ21=HZ21*CEXP(-CJ*2.*PI*D*SPHS)
      HZ421=HZ421*PHASS
C CALC DOUBLE DIFFRACTION FROM RESISTIVE TO MATERIAL H-P
      SGNS=1.
      SGNI=1.
      CALL DOUB21(HZ12,PHI,PHS,D,M,SGNI,SGNS)
      HZ12=HZ12*CEXP(-CJ*2.*PI*D*SPHI)
      CALL QUAD(HZ412,PHI,PHS,D,2,SGNI,SGNS)
      HZ412=HZ412*PHASI
      SGNI=1.
      SGNS=1.
      CALL TRIP1(HZ121,PHS,PHI,D,1,SGNS,SGNI)
      CALL QUINT1(HZ51,PHS,PHI,D,1,SGNS,SGNI)
      SGNS=1.
      SGNI=1.
      CALL TRIP2(HZ212,PHI,PHS,D,M,SGNI,SGNS)
      CALL QUINT1(HZ52,PHI,PHS,D,2,SGNI,SGNS)
      HZ212=HZ212*PHASI*PHASS
      HZ52=HZ52*PHASI*PHASS
11    ANG(I)=PHS*180./PI
      PHI=PHI+DPHI
      PHS=PHS+DPHS
      TEMPC=HZ1+HZ2+HZ21+HZ12
      IF(M2.EQ.5)TEMPC=TEMPC+HZ51+HZ52+HZ421+HZ412+HZ121+HZ212
      IF(IPRINT.EQ.1) THEN
       PRINT *,(PHI-dphi),(PHS-DPHS)*180/PI,HZ1,HZ2
       PRINT *,HZ2+HZ12,HZ21+HZ121,HZ212+HZ412
       PRINT *,HZ421+HZ51,HZ52
C        PRINT *,'HZ421,HZ51:',HZ421,HZ51
       PRINT *,HZ21,HZ12,HZ121,HZ212,HZ421,HZ412
      ENDIF
      TEMPC=2.*PI*TEMPC*TEMPC
      HZ(I)=10*ALOG10(CABS(TEMPC))
      PHASE=ATAN2(AIMAG(TEMPC),REAL(TEMPC))*180./PI
      PRINT *,'ANG,HZ: ',ANG(I),HZ(I),TEMPC
      WRITE(2,100) ANG(I),HZ(I),PHASE
C100   FORMAT(F10.5,'*',F10.5,'*',2F10.5,'*',F10.5)
100   FORMAT(2F8.3,F8.2)
1000  CONTINUE
```

```
      IEND=0
      IF(IPLOT.EQ.NPLOT)IEND=1
      CALL GENPLO(ANG,HZ,NPTS,IPLOT-1,IEND)
 2000 CONTINUE
      CALL EXIT
      END
C ****************
      SUBROUTINE HZ1M(HZ1,PHI,PHS)
      COMMON /BLK1/ETA1,ETAR,ETAS,ETAES,ETAMS,ETAM1,ETAM2,CON1,CON2
      COMMON /BLK2/CJ,CJ4,PI,PI2
      COMPLEX KPLUS1,KPLUS2,KPLUS3,KPLUS4,KPLUS5,KPLUS6
      COMPLEX KPLUSM,KPLUSP,CON1,CON2
      COMPLEX ETA1,ETAS,ETAR,ETAES,ETAMS,ETAM1,ETAM2
      COMPLEX CJ,CJ4,HZE,HZR,HZM1,HZM2,HZ1,TU,TL,RU,RL
      COMMON /REFL/RU,RL,TU,TL
      KPLUS1=KPLUSM(CMPLX(PHS,0.),ETA1,0,1.)
      KPLUS2=KPLUSM(CMPLX(PHI,0.),ETA1,0,1.)
      KPLUS3=KPLUSM(CMPLX(PHS,0.),ETAM1,0,1.)
      KPLUS4=KPLUSM(CMPLX(PHI,0.),ETAM1,0,1.)
      KPLUS5=KPLUSM(CMPLX(PHS,0.),ETAM2,0,1.)
      KPLUS6=KPLUSM(CMPLX(PHI,0.),ETAM2,0,1.)
      TEMP1=1./COS((PHI+PHS)/2.)
      TEMP2=1./COS((PHI-PHS)/2.)
      TEMP=TEMP1+TEMP2
      SPHI=SIN(PHI)
      SPHS=SIN(PHS)
      CPHI=COS(PHI)
      CPHS=COS(PHS)
      HZE=-CJ4*KPLUS1*KPLUS2*TEMP*ETA1/(4.*PI)
      KPLUSP=KPLUS3*KPLUS4*KPLUS5*KPLUS6
      HZM2=-CJ4*ETAS*KPLUSP*TEMP*CPHI*CPHS/(4.*PI*ETAES*SPHI*SPHS)
      HZM1=CJ4*ETAS*KPLUSP*TEMP/(4.*PI*SPHI*SPHS*ETAMS)
      HZ1=HZE+HZM1+HZM2
      RETURN
      END
C ****************
      SUBROUTINE HZ1R(HZ1,PHI,PHS)
      COMMON /BLK1/ETA1,ETAR,ETAS,ETAES,ETAMS,ETAM1,ETAM2,CON1,CON2
      COMMON /BLK2/CJ,CJ4,PI,PI2
      COMMON /REFL/RU,RL,TU,TL
      COMPLEX KPLUSM,KPLUSP,KPLUS7,KPLUS8,CON1,CON2
      COMPLEX ETA1,ETAS,ETAR,ETAES,ETAMS,ETAM1,ETAM2
      COMPLEX CJ,CJ4,HZR,HZ1,RU,TU,RL,TL
      KPLUS7=KPLUSM(CMPLX(PHS,0.),ETAR,0,1.)
      KPLUS8=KPLUSM(CMPLX(PHI,0.),ETAR,0,1.)
      TEMP1=1./COS((PHI+PHS)/2.)
      TEMP2=1./COS((PHI-PHS)/2.)
      TEMP=TEMP1+TEMP2
      SPHI=SIN(PHI)
      SPHS=SIN(PHS)
      HZR=-CJ4*KPLUS7*KPLUS8*TEMP*ETAR/(4.*PI)
      HZ1=HZR
      RETURN
      END
C **************************
      SUBROUTINE DOUB21(HZ21,PHS,PHI,W,M,S1,S2)
C DOUBLE DIFFRACTION FROM MATERIAL TO RESISTIVE HALF PLANE
      COMMON /BLK1/ETA1,ETAR,ETAS,ETAES,ETAMS,ETAM1,ETAM2,COM1,COM2
      COMMON /BLK2/CJ,CJ4,PI,PI2
      COMMON /REFL/RU,RL,TU,TL,PHASS,PHASI
```

```
      COMPLEX ETA1,ETAS,ETAR,ETAES,ETAMS,ETAM1,ETAM2,COM1,COM2
      COMPLEX CJ,CJ4,HZE,HZR,HZM1,HZM2,HZ21,RU,RL,RM,RM1,RM2,RMM
      COMPLEX DEL,FFUN,FI,tt,TU,TL,PHASS,PHASI
C      DEL=CJ4*CJ4/(16*PI*PI)
      DEL=(1.,0.)
      RM=.25*CEXP(-CJ*4.*PI*W)
      RMM=(1.,0.)
C      GO TO 200
C      M=10
      DO 100 N=4,M,2
      N1=N-2
      RM1=CEXP(-CJ*N1*2.*PI*W)/(2.**N1)
      N2=(N-2+.0001)/2.
      RM2=(1.,0.)
      DO 10 I=1,N2
10    RM2=RM2*RU*RL
100   RMM=RM1*RM2+RMM
200   CONTINUE
C      PRINT *,'RMM IN HZ12:',RMM,RM*RU*RL,N1,N2
C     RMM=(1.,0.)
      DEL=DEL*CEXP(-CJ*2.*PI*W)/SQRT(W)
      AL1=1.5*PI-PHI
      AL2=1.5*PI+PHI
      AL3=-PI2-PHS
      AL4=-PI2+PHS
C      TEMP=(1./COS(.5*AL1))+(1./COS(.5*AL2))
C      TEMPC=(1./COS(.5*AL3))+(1./COS(.5*AL4))
      HZ21=S1*FI(AL1,AL3,W)+FI(AL1,AL4,W)
      HZ21=HZ21+S1*S2*FI(AL2,AL3,W)+S2*FI(AL2,AL4,W)
      HZ21=HZ21*DEL*FFUN(PHS,PHI,0)
      HZ21=HZ21*RMM
      RETURN
      END
C ************************
      SUBROUTINE TRIP1(HZ121,PHS,PHI,W,M,S1,S2)
C TRIPLE DIFFRACTION FROM MATERIAL TO RESISTIVE HALF PLANE
      COMMON /BLK1/ETA1,ETAR,ETAS,ETAES,ETAMS,ETAM1,ETAM2,COM1,COM2
      COMMON /BLK2/CJ,CJ4,PI,PI2
       COMMON /REFL/RU,RL,TU,TL
      COMPLEX ETA1,ETAS,ETAR,ETAES,ETAMS,ETAM1,ETAM2,COM1,COM2
      COMPLEX CJ,CJ4,HZE,HZR,HZM1,HZM2,HZ121,RU,RL,RMM,RM1,RM2,RM
      COMPLEX DEL,FFUN,FI,FIP,T1,T2,TT,FFCT,TT1,DEL1,TU,TL
      DATA RT2/1.414213562/
      DEL=CEXP(-2.*PI*CJ*W)/SQRT(W)
      DEL1=(4.*16*PI*PI*PI)/(CJ4*CJ4*CJ4)
      IF(M.EQ.1) THEN
       HZ121=-FFUN(PHS,PHS,1)*FFUN(PHI,PHI,1)*FFUN(PI2,PI2,2)
      ELSE
       HZ121=-FFUN(PHS,PHS,2)*FFUN(PHI,PHI,2)*FFUN(PI2,PI2,1)
      ENDIF
      HZ121=DEL*DEL*HZ121
      AL1=1.5*PI-PHI
      AL2=1.5*PI+PHI
      AL3=-1.5*PI+PHS
      AL4=-1.5*PI-PHS
      TT=FI(AL1,AL3,W)+S1*FI(AL1,AL4,W)
      TT=TT+S1*FI(AL2,AL3,W)+S1*S2*FI(AL2,AL4,W)
      TT1=-2.*PI*SQRT(W)*CJ*CJ4*TT
      TT=(FI(0.,AL1,W)+S2*FI(0.,AL2,W))
      TT=TT*(FI(0.,AL3,W)+S1*FI(0.,AL4,W))
```

```
C      TT=(0.,0.)
      IF(M.NE.1)PRINT *,'ALS,TT1,TT:',AL1,AL2,AL3,AL4,TT1,TT
      HZ121=HZ121*(TT1+TT)
      RETURN
      END
C *****************************
      SUBROUTINE TRIP2(HZ212,PHS,PHI,W,M,S1,S2)
C TRIPLE DIFFRACTION FROM MATERIAL TO RESISTIVE HALF PLANE
      COMMON /BLK1/ETA1,ETAR,ETAS,ETAES,ETAMS,ETAM1,ETAM2,COM1,COM2
      COMMON /BLK2/CJ,CJ4,PI,PI2
      COMMON /REFL/RU,RL
      COMPLEX ETA1,ETAS,ETAR,ETAES,ETAMS,ETAM1,ETAM2,COM1,COM2
      COMPLEX CJ,CJ4,HZE,HZR,HZM1,HZM2,HZ212,RU,RL,RMM,RM1,RM2,RM
      COMPLEX DEL,FFUN,FI,FIP,T1,T2,TT,FFCT,TT1,DEL1
      DATA RT2/1.414213562/
      DEL=CEXP(-2.*PI*CJ*W)/SQRT(W)
      HZ212=FFUN(PHS,PHS,2)*FFUN(PHI,PHI,2)
      HZ212=DEL*HZ212
      TT1=HZ212*DEL*FFUN(1.5*PI,1.5*PI,1)
      RM=.5*RU*CEXP(-2.*PI*CJ*W)
      RMM=(0.,0.)
      RM1=(0.,0.)
C      M=11
      DO 100 N=3,M,2
       N1=N-3
       RM1=CEXP(-CJ*N1*2.*PI*W)/(2.**N1)
       N2=(N-3+.0001)/2.
       RM2=(1.,0.)
       DO 10 I=1,N2
 10    RM2=RM2*RU*RL
100   RMM=RM1*RM2*RM+RMM
c     PRINT *,'RMM:',RMM,.5*RL*CEXP(-2.*PI*CJ*W)
      AL1=-.5*PI+PHI
      AL2=-.5*PI-PHI
      AL3=-.5*PI+PHS
      AL4=-.5*PI-PHS
      TT=FI(AL1,AL3,W)+S1*FI(AL1,AL4,W)
      TT=TT+S2*FI(AL2,AL3,W)+S1*S2*FI(AL2,AL4,W)
C     PRINT *,'FIS IN 121:',TT,HZ212,(CJ4/(4.*PI))*(CJ4/(4.*PI))
      HZ212=HZ212*TT*RMM
      TT=FI(0.,AL1,W)+S2*FI(0.,AL2,W)
      TT=TT*(FIP(0.,AL3,W)*SEC(AL3/2.)+S1*FIP(0.,AL4,W)*SEC(AL4/2.))
C      PRINT *,'AL,TT:',AL1,AL2,AL3,AL4,TT
      TT=TT1*TT
      HZ212=HZ212-TT
      RETURN
      END
C *************************
      SUBROUTINE QUAD(HZ4,PHS,PHI,W,M,S1,S2)
C QUADRUPLE DIFFRACTION FROM RESISTIVE/MATERIAL HALF PLANE
      COMMON /BLK1/ETA1,ETAR,ETAS,ETAES,ETAMS,ETAM1,ETAM2,COM1,COM2
      COMMON /BLK2/CJ,CJ4,PI,PI2
      COMPLEX ETA1,ETAS,ETAR,ETAES,ETAMS,ETAM1,ETAM2,COM1,COM2
      COMPLEX CJ,CJ4,HZE,HZR,HZ4,KPLUS7,KPLUS8,KPLUSM
      COMPLEX DEL,FFUN,FI,FI1,FIP,T1,T2,TT,FFCT,TT1,DEL1,IA
      DATA RT2/1.414213562/
      DEL=CEXP(-6.*PI*CJ*W)/(W*SQRT(W))
      KPLUS7=KPLUSM(CMPLX(PI2,0.),ETAR,0,1.)
      HZR=CJ4*ETAR*KPLUS7*KPLUS7/(4.*PI)
      HZ4=FFUN(PHS,1.5*PI,0)*FFUN(PHS,PHI,1)
```

```
      HZ4=HZ4*HZR
      HZ4=DEL*HZ4
      DEL1=HZ4
      AL4=-PI2-PHS
      AL3=PHS-PI2
      AL11=1.5*PI-PHI
      AL12=1.5*PI+PHI
      IF(M.EQ.1) THEN
       IF(PHS.GT.PI2)AL=-PI+.01
       IF(PHS.LT.PI2)AL=-PI-.01
      ELSE
       IF(PHI.GT.PI2)AL=-PI-.01
       IF(PHI.LT.PI2)AL=-PI+.01
      ENDIF
      IA=FI(AL3,0.,W)+S1*FI(AL4,0.,W)
      T2=-2.*PI*SQRT(W)*CJ*CJ4
      T1=T2*IA
      TT=FI(AL11,0.,W)+S2*FI(AL12,0.,W)
      T1=2*T1*TT
      TT=FI(AL3,AL11,W)+S2*FI(AL3,AL12,W)
      TT=TT+S1*FI(AL4,AL11,W)+S1*S2*FI(AL4,AL12,W)
      T2=T2*T2*TT
      HZ4=DEL1*(T1+T2)
      TT=FI(AL3,0.,W)+S1*FI(AL4,0.,W)
      T1=FI(0.,0.,W)*(FI(0.,AL11,W)+S2*FI(0.,AL12,W))
C      PRINT *,'QUAD:',TT,T1
      T1=T1+FI(AL,0.,W)*(FI1(AL11,W)+S2*FI1(AL12,W))
C      PRINT *,'QUAD:',AL,AL11,AL12,AL3,AL4,T1
      HZ4=HZ4+DEL1*(TT*T1)
      RETURN
      END
C ************************
      SUBROUTINE QUINT1(HZ51,PHS,PHI,W,M,S1,S2)
C QUINTAPLE DIFFRACTION FROM RESISTIVE/MATERIAL HALF PLANE
      COMMON /BLK1/ETA1,ETAR,ETAS,ETAES,ETAMS,ETAM1,ETAM2,COM1,COM2
      COMMON /BLK2/CJ,CJ4,PI,PI2
      COMPLEX ETA1,ETAS,ETAR,ETAES,ETAMS,ETAM1,ETAM2,COM1,COM2
      COMPLEX CJ,CJ4,HZE,HZR,HZ51,KPLUS7,KPLUS8,KPLUSM
      COMPLEX DEL,FFUN,FI,FI1,FIP,T1,T2,TT,FFCT,TT1,DEL1,IA,IB,IC,ID
      DATA RT2/1.414213562/
      DEL=CEXP(-2.*PI*CJ*W)/(SQRT(W))
C      KPLUS7=KPLUSM(CMPLX(PI2,0.),ETAR,0,1.)
C      HZR=CJ4*ETAR*KPLUS7*KPLUS7/(4.*PI)
      Q1=1.
      Q2=1.
      P1=1.
      P2=1.
      IF(M.EQ.1) THEN
       HZ51=FFUN(PI2,1.5*PI,0)*FFUN(PI2,PHS,1)*FFUN(PI2,PI2,2)
       HZ51=-HZ51*FFUN(PI2,PHI,1)
       Q1=S1
       Q2=S2
      ELSE
       HZ51=FFUN(1.5*PI,.5*PI,0)*FFUN(PI2,PHS,2)*FFUN(PI2,PI2,1)
       HZ51=-HZ51*FFUN(PI2,PHI,2)
       P1=S1
       P2=S2
      ENDIF
      DEL1=CJ4/(4.*PI)
      HZ51=DEL*DEL*DEL*DEL*HZ51
```

```
      AL1=1.5*PI-PHI
      AL2=1.5*PI+PHI
      AL3=1.5*PI-PHS
      AL4=1.5*PI+PHS
      IF(M.EQ.1) THEN
       IF(PHS.GT.PI2)AL=-PI+.01
       IF(PHS.LT.PI2)AL=-PI-.01
      ELSE
       IF(PHI.GT.PI2)AL=-PI-.01
       IF(PHI.LT.PI2)AL=-PI+.01
      ENDIF
      IA=P1*FI(0.,AL3,W)+Q1*FI(0.,AL4,W)
      T2=-2.*PI*SQRT(W)*CJ*CJ4
      IB=FI(AL,0.,W)*(P2*FI1(AL1,W)+Q2*FI1(AL2,W))
      IB=IB+FI(0.,0.,W)*(P2*FI(0.,AL1,W)+Q2*FI(0.,AL2,W))
      T1=T2*IA*IB
C      PRINT *,'T1:1',T1,IA,IB,FI(0.,0.,W)
      IA=T2*(P2*P1*FI(AL1,AL3,W)+P2*Q1*FI(AL1,AL4,W)+
     &Q2*P1*FI(AL2,AL3,W)+Q2*Q1*FI(AL2,AL4,W))
      IB=(P2*FI(0.,AL1,W)+Q2*FI(0.,AL2,W))
      IB=IB*(P1*FI(0.,AL3,W)+Q1*FI(0.,AL4,W))
      T1=T1+T2*T2*(IA+IB)
C      PRINT *,'T1:3:',T1,IA,IB
C      HZ51=HZ51*T1
CC      PRINT *,'HZ51:',HZ51
      IA=FI(AL,0.,W)*(P1*FI1(AL3,W)+Q1*FI1(AL4,W))
      IB=FI(0.,0.,W)*(P1*FI(AL3,0,W)+Q1*FI(AL4,0.,W))
      IC=FI(AL,0.,W)*(Q1*FI1(AL1,W)+Q2*FI1(AL2,W))
      ID=FI(0.,0.,W)*(Q1*FI(AL1,0.,W)+Q2*FI(AL2,0.,W))
      T1=T1+(IA+IB)*(IC+ID)
C      PRINT *,'T1:4:',T1,IA,IB,IC,ID
      HZ51=HZ51*T1
      RETURN
      END
C ************************
      REAL FUNCTION SEC(X)
      SEC=1./COS(X)
      RETURN
      END
C *************************
      COMPLEX FUNCTION FFUN(PHS,PHI,IC)
      COMPLEX ETA1,ETAS,ETAR,ETAES,ETAMS,ETAM1,ETAM2,COM1,COM2
      COMPLEX KPLUSM,KPLUS1,KPLUS2,KPLUS7,KPLUS8,KPLUSP
      COMPLEX KPLUS3,KPLUS4,KPLUS5,KPLUS6
      COMPLEX CJ,CJ4,HZE,HZR,HZM1,HZM2,HZM
      COMMON /BLK1/ETA1,ETAR,ETAS,ETAES,ETAMS,ETAM1,ETAM2,COM1,COM2
      COMMON /BLK2/CJ,CJ4,PI,PI2
      DATA RT2/1.414213562/
      IF(IC.EQ.2)GO TO 110
      KPLUS1=KPLUSM(CMPLX(PI2,0.),ETA1,0,1.)
      KPLUS2=KPLUSM(CMPLX(PHI,0.),ETA1,0,1.)
      KPLUS3=KPLUSM(CMPLX(PI2,0.),ETAM1,0,1.)
      KPLUS4=KPLUSM(CMPLX(PHI,0.),ETAM1,0,1.)
      KPLUS5=KPLUSM(CMPLX(PI2,0.),ETAM2,0,1.)
      KPLUS6=KPLUSM(CMPLX(PHI,0.),ETAM2,0,1.)
      SPHS=SIN(PI2)
      SPHI=SIN(PHI)
      HZE=CJ4*ETA1*KPLUS1*KPLUS2/(4.*PI)
      KPLUSP=KPLUS3*KPLUS4*KPLUS5*KPLUS6
      HZM2=CJ4*ETAS*KPLUSP*COS(PHI)*COS(PI2)/(4.*PI*ETAES*SPHI*SPHS)
```

```
      HZM1=-CJ4*ETAS*KPLUSP/(4.*PI*SPHI*SPHS*ETAMS)
      HZM=HZM1+HZM2
C       PRINT *,'IC:',IC
      HZR=(1.,0.)
      IF(IC.EQ.0)THEN
       KPLUS7=KPLUSM(CMPLX(PHS,0.),ETAR,0,1.)
       KPLUS8=KPLUSM(CMPLX(PI2,0.),ETAR,0,1.)
       HZR=CJ4*ETAR*KPLUS7*KPLUS8/(4.*PI)
      ENDIF
      FFUN=(HZE-HZM)*HZR
      GO TO 100
110   KPLUS7=KPLUSM(CMPLX(PHS,0.),ETAR,0,1.)
      KPLUS8=KPLUSM(CMPLX(PI2,0.),ETAR,0,1.)
      FFUN=CJ4*ETAR*KPLUS7*KPLUS8/(4.*PI)
100   RETURN
      END
C  ****************************
      COMPLEX FUNCTION FI(AL1,AL2,W)
      COMPLEX FIP
      TEMP=1./(COS(.5*AL1)*COS(.5*AL2))
      FI=TEMP*FIP(AL1,AL2,W)
C     fi=temp
      RETURN
      END
C *****************************
      COMPLEX FUNCTION FI1(AL1,W)
      COMPLEX FFCT
      DATA RT2,PI/1.414213562,3.141592654/
      TEMP=1./COS(.5*AL1)
      A1=RT2/TEMP
      A1=A1*A1
      FI1=TEMP*FFCT(2.*PI*W*A1)
      RETURN
      END
C ******************************
      COMPLEX FUNCTION FIP(AL1,AL2,W)
      COMPLEX FFCT,fip1
      DATA RT2,PI/1.414213562,3.141592654/
      A11=RT2*COS(0.5*AL1)
      A22=RT2*COS(0.5*AL2)
      A1=A11*A11
      A2=A22*A22
      IF(A1.EQ.A2) THEN
       TEMP=2.*PI*W*A1
       FIP1=FFCT(2.*PI*W*A1)
       FIP=-(0.,1.)*TEMP*(FIP1-1.)
       FIP=FIP+.5*FIP1
C        PRINT *,'FIP:',FIP
       RETURN
      ENDIF
      END
```